Published in final edited form as:

Nat Med. 2020 March ; 26(3): 398–407. doi:10.1038/s41591-020-0781-z.

A soluble phosphorylated tau signature links tau, amyloid and the evolution of stages of dominantly inherited Alzheimer's disease

Nicolas R. Barthélemy[1], **Yan Li**[1,2], **Nelly Joseph-Mathurin**[3], **Brian A. Gordon**[3], **Jason Hassenstab**[1], **Tammie. L. S. Benzinger**[3], **Virginia Buckles**[1], **Anne M. Fagan**[1], **Richard J. Perrin**[4], **Alison M. Goate**[5], **John C. Morris**[1], **Celeste M. Karch**[6], **Chengjie Xiong**[2], **Ricardo Allegri**[7], **Patricio Chrem Mendez**[7], **Sarah B. Berman**[8], **Takeshi Ikeuchi**[9], **Hiroshi Mori**[10], **Hiroyuki Shimada**[10], **Mikio Shoji**[11], **Kazushi Suzuki**[12], **James Noble**[13], **Martin Farlow**[14], **Jasmeer Chhatwal**[15], **Neill R. Graff-Radford**[16], **Stephen Salloway**[17,18], **Peter R. Schofield**[19,20], **Colin L. Masters**[21,22], **Ralph N. Martins**[23], **Antoinette O'Connor**[24], **Nick C. Fox**[24], **Johannes Levin**[25,26,27], **Mathias Jucker**[28,29], **Audrey Gabelle**[30], **Sylvain Lehmann**[30], **Chihiro Sato**[1], **Randall J. Bateman**[1,✉], **Eric McDade**[1,✉], **Dominantly Inherited Alzheimer Network**[*]

[1]Department of Neurology, Washington University School of Medicine, Saint Louis, MO, USA

✉**Correspondence and requests for materials** should be addressed to R.J.B. or E.M. batemanr@wustl.edu; ericmcdade@wustl.edu.
*A list of members and affiliations appears at the end of the paper.

Author contributions

N.R.B. and C.S. performed the mass spectrometry analyses. Y.L., C.X., N.J.-M. and B.A.G. performed the statistical and imaging analyses. N.R.B., Y.L., R.J.B. and E.M. designed the study and wrote the initial draft of the manuscript. All authors collected samples and data, helped to interpret the results and reviewed drafts of the manuscript.

Competing interests

R.J.B. has equity ownership interest in C2N Diagnostics and receives royalty income based on technology (stable isotope labeling kinetics and blood plasma assay) licensed by Washington University to C2N Diagnostics. R.J.B. receives income from C2N Diagnostics for serving on the scientific advisory board. Washington University, with R.J.B., E.M. and N.R.B. as co-inventors, has submitted the US nonprovisional patent application 'Cerebrospinal fluid (CSF) tau rate of phosphorylation measurement to define stages of Alzheimer's disease and monitor brain kinases/phosphatases activity'. R.J.B. has received honoraria from Janssen and Pfizer as a speaker, and from Merck and Pfizer as an advisory board member. E.M. has received royalty payments for an educational program supported by Eli Lilly and as a member of a scientific advisory board for Eli Lilly.

Extended data is available for this paper at https://doi.org/10.1038/s41591-020-0781-z.

Supplementary information is available for this paper at https://doi.org/10.1038/s41591-020-0781-z.

Peer review information Brett Benedetti and Kate Gao were the primary editors on this article and managed its editorial process and peer review in collaboration with the rest of the editorial team.

Reporting Summary. Further information on research design is available in the Nature Research Reporting Summary linked to this article.

Data availability

The data that support the findings of this study can be requested from DIAN at https://dian.wustl.edu/our-research/observational-study/dian-observational-study-investigator-resources/.

Code availability

All codes used for data analyses are available upon request from the corresponding authors.

Online content

Any methods, additional references, Nature Research reporting summaries, source data, extended data, supplementary information, acknowledgements, peer review information; details of author contributions and competing interests; and statements of data and code availability are available at https://doi.org/10.1038/s41591-020-0781-z.

Publisher's note Springer Nature remains neutral with regard to jurisdictional claims in published maps and institutional affiliations.

[2]Division of Biostatistics, Washington University School of Medicine, Saint Louis, MO, USA

[3]Department of Radiology, Washington University School of Medicine, Saint Louis, MO, USA

[4]Department of Pathology, Washington University School of Medicine, Saint Louis, MO, USA

[5]Department of Neuroscience, Icahn School of Medicine at Mount Sinai, New York, NY, USA

[6]Department of Psychiatry, Washington University School of Medicine, Saint Louis, MO, USA

[7]Fundación para la Lucha contra las Enfermedades Neurológicas de la Infancia (FLENI) Instituto de Investigaciones Neurológicas Raúl Correa, Buenos Aires, Argentina.

[8]University of Pittsburgh School of Medicine, Pittsburgh, PA, USA

[9]Niigata University, Niigata, Japan

[10]Osaka City University, Osaka, Japan

[11]Hirosaki University, Hirosaki, Japan

[12]Tokyo University, Tokyo, Japan

[13]Columbia University, College of Physicians and Surgeons, New York, NY, USA

[14]Department of Neurology, Indiana University, Indianapolis, IN, USA

[15]Massachusetts General Hospital, Harvard Medical School, Boston, MA, USA

[16]Department of Neurology, Mayo Clinic Jacksonville, Jacksonville, FL, USA

[17]Butler Hospital, Providence, RI, USA

[18]Brown University, Providence, RI, USA

[19]Neuroscience Research Australia, Sydney, New South Wales, Australia

[20]School of Medical Sciences, University of New South Wales, Sydney, New South Wales, Australia

[21]The Florey Institute of Neuroscience and Mental Health, Melbourne, Victoria, Australia

[22]University of Melbourne, Melbourne, Victoria, Australia

[23]Edith Cowan University, Perth, Western Australia, Australia

[24]Dementia Research Centre, Institute of Neurology, University College London, London, UK

[25]German Center for Neurodegenerative Diseases (DZNE) Munich, Munich, Germany

[26]Department of Neurology, Ludwig-Maximilians Universität München, Munich, Germany

[27]Munich Cluster for Systems Neurology (SyNergy), Munich, Germany

[28]German Center for Neurodegenerative Diseases (DZNE), Tübingen, Germany

[29]Hertie-Institute for Clinical Brain Research, University of Tübingen, Tübingen, Germany

[30]Laboratoire de Biochimie et Protéomique Clinique and CRB, INSERM-UM, CHU Montpellier, Montpellier, France, Montpellier, France

Abstract

Development of tau-based therapies for Alzheimer's disease requires an understanding of the timing of disease-related changes in tau. We quantified the phosphorylation state at multiple sites of the tau protein in cerebrospinal fluid markers across four decades of disease progression in dominantly inherited Alzheimer's disease. We identified a pattern of tau staging where site-specific phosphorylation changes occur at different periods of disease progression and follow distinct trajectories over time. These tau phosphorylation state changes are uniquely associated with structural, metabolic, neurodegenerative and clinical markers of disease, and some (p-tau217 and p-tau181) begin with the initial increases in aggregate amyloid-β as early as two decades before the development of aggregated tau pathology. Others (p-tau205 and t-tau) increase with atrophy and hypometabolism closer to symptom onset. These findings provide insights into the pathways linking tau, amyloid-β and neurodegeneration, and may facilitate clinical trials of tau-based treatments.

The microtubule-associated protein tau (MAPT or τ) plays an essential role in the morphology and physiology of neurons[1,2]. Phosphorylation is an important post-translational modification for regulating the normal function of tau in axonal stabilization, and can occur at over 80 different positions[3]. However, excessive phosphorylation of tau (p-tau) appears to increase the probability of tau aggregating into intracellular insoluble paired helical filaments and neurofibrillary tangles (NFTs)[4,5], which are primarily composed of hyperphosphorylated tau. Intracellular NFTs in the cerebral cortex are a defining pathological feature of Alzheimer's disease (AD) and correlate with the onset of clinical symptoms long after the appearance of extracellular aggregated amyloid-β (Aβ) 'plaques'[6,7], which begin to develop up to two decades before symptom onset[8,9]. In AD, soluble p-tau181 (pT181) and t-tau are elevated in the cerebrospinal fluid (CSF)[10–12] and begin to increase before symptom onset in both dominantly inherited AD (DIAD) and sporadic AD (sAD)[13,14]. It has been proposed that these changes reflect the effects of neuronal death (neurodegeneration) passively releasing tau and NFTs[15,16] into the CSF. However, in other tauopathies with significant NFT pathology and neurodegeneration (for example, progressive supranuclear palsy and frontotemporal lobar degeneration-tau), CSF levels of soluble pT181 and t-tau do not increase[17,18], and in AD, NFTs measured by tau positron emission tomography (tau-PET) only modestly correlate with CSF t-tau and p-tau[19,20]. Moreover, recent work in DIAD and sAD has suggested that NFTs, as measured by tau-PET, primarily increase at symptom onset 10–15 years after[21–25] soluble tau increase[9,26,27]. Furthermore, the rate of the increase of p-tau and tau levels may actually slow as neurodegeneration increases[8,13,28]. These observations suggest that the tauopathy of AD is a more dynamic process than is currently conceptualized[15], that soluble and aggregated tau probably have important differences, and that cerebral Aβ may trigger a process that leads to the unique tauopathy of AD[22,29–37]. This concept is further supported by an increase in the active production of soluble tau in the presence of aggregated amyloid in humans[33]. ^{11}C-Pittsburgh compound B (PiB)-PET imaging of cortical aggregated Aβ has detected Aβ pathology two decades before the appearance of symptoms in DIAD[8,38], but has not consistently been linked with a rise in CSF tau and pT181 (ref. [8]). However, unresolved questions include: 'what is the relationship of tau to aggregated Aβ?' and 'what

are the different tau pathophysiological changes that occur during the preclinical and clinical stages of AD?'. The answers to these questions will help identify the tau pathophysiological processes that are related to AD and neurodegeneration, which is a critical step needed to advance therapeutic and diagnostic targets for the disease.

An important limitation to understanding the tauopathy of AD has been the lack of methods that can simultaneously quantify phosphorylation at multiple positions of the tau protein in a population representing the full clinicopathological spectrum of AD (that is, from 'at risk' to dementia). To further explore these questions and limitations, we developed a mass spectrometry method to measure the phosphorylation occupancy (phosphorylated to unphosphorylated) at multiple tau phosphorylation sites in the proline-rich protein domain ranging from 150–220 residues[33] in CSF, independent of variation in t-tau levels. We measured CSF from a large cohort of comprehensively studied participants with DIAD (n = 370), as well as a cohort of adult participants either with sAD or with unaffected cognition but a risk of disease (based on the presence of abnormal Aβ pathology) (n = 104) (Table 1 and Supplementary Table 1). We quantified multiple positions throughout tau and the associated phosphorylation occupancy to determine disease stage-specific changes in soluble p-tau isoforms. The relatively predictable age of disease onset in DIAD families[39] enables us to infer the pattern of change across decades of AD progression. This cohort was recruited and evaluated by the Dominantly Inherited Alzheimer Network (DIAN)—a global, multi-site, observational study of adults with, and at risk of carrying, causative mutations for early-onset AD. Participants undergo a comprehensive, standardized assessment of biofluids and brain imaging, with cognitive and clinical assessments.

The results of our investigation show that hyperphosphorylation at specific sites of the tau protein is a dynamic process that changes first based on the pathological state (that is, the presence and amount of aggregated Aß) and then based on the stage of disease and clinical stage (cognitively normal or cognitively impaired) of AD in both DIAD and sAD. Furthermore, in DIAD, we demonstrate that these phosphorylation sites have opposite trajectories of change at different stages over the 30 years of the DIAD process and have different associations with brain hypometabolism, atrophy and cognitive decline (Fig. 1). These findings suggest a predictable progression of changes in tau phosphorylation (an AD-tau staging system) and support recent tau kinetic studies demonstrating aggregated Aß-related active release of phosphorylated tau[33]. Moreover, this AD-tau staging suggests potential tau targets for the development of tau-specific therapeutics and provides downstream measures for therapies targeting early amyloid pathology.

Results

Disease stage and progression are associated with site-specific differences in tau hyperphosphorylation and longitudinal rates of change in DIAD and sAD

The certainty of disease and predictability of symptom onset of DIAD enables the staging of individuals based on the estimated years to symptom onset (EYO)[8,9,26] (that is, the age of an individual at the time of assessment relative to the age of onset of others with the mutation). Therefore, we determined whether there were temporal differences in the pattern of phosphorylation of CSF tau as it relates to the EYO. This was done by estimating the

differences in the amount and rate of change in phosphorylation over time between mutation carriers and non-carriers based on the EYO. There were two important findings. First, there was evidence that increases in t-tau and phosphorylation at specific sites occurred in a relative order: phosphorylation of tau at threonine 217 (pT217/T217) (which occurred at around −21 EYO) was followed by that of threonine 181 (pT181/T181) (−19 EYO), then t-tau increase (−17 EYO), then phosphorylation of tau at threonine 205 (pT205/T205) (−13 EYO) (Fig. 2, Extended Data Fig. 1a–e and Supplementary Table 2). The initial increase of pT217/T217, and to a lesser extent in pT181/T181, occurred at a similar time to when PiB-PET SUVR began to increase (−19 EYO) (see below).

Second, pT217/T217 and pT181/T181 began to decline significantly near the time of symptom onset, while phosphorylation at pT205/T205 slowed and t-tau levels continued to increase. Of note, the concentrations of all of the corresponding unphosphorylated isoforms (T181, S202/T205 and T217) increased with disease progression, suggesting that the decrease in the phosphorylation ratio for pT217/T217 and pT181/T181 was not a result of a disproportionate rise in unphosphorylated peptides specifically related to these two sites, nor a decrease in total levels of tau protein (Extended Data Fig. 2). At the 202 position of serine (pS202/S202), there was no significant change in phosphorylation over the course of the disease (Fig. 2 and Extended Data Fig. 2c).

Next, we assessed whether the above findings were also seen in an elderly group of patients with sAD and non-carriers who were at risk for AD, based on the presence of abnormal Aβ biomarkers (preclinical AD (n = 63)) or normal Aβ biomarkers (n = 39). This group of participants underwent the following clinical assessments: the Clinical Dementia Rating (CDR) scale, CSF collection and Aβ measures cross-sectionally. Because sAD is associated with a later age and additional pathologies (for example, higher vascular disease burden and greater TAR DNA-binding protein 43 inclusions) compared with a more ‘pure’ form of AD in DIAD, it is possible that there could be important differences in tau phosphorylation between the two types of AD. However, the preclinical sAD population lacked a predictor of disease onset similar to EYO in DIAD, and longitudinal CSF data were not available; therefore, we compared the two groups based on: (1) the absence or presence of amyloid pathology (to define a similar AD risk state); and (2) the stage of dementia symptoms, using the CDR (where CDR 0 = no dementia, CDR 0.5 = very mild dementia and CDR ≥ 1 = mild to moderate dementia)[40] (Fig. 3c).

Overall, there was a similar pattern of phosphorylation changes at each site for both cohorts. In both DIAD and sAD, pT217/T217 and pT181/T181 ratios increase significantly with the presence of amyloid pathology and then less so with more advanced stages of symptoms. However, the rate of phosphorylation of T205 and levels of t-tau increase at later stages and continue increasing as clinical disease progresses. Similarly, in both DIAD and sAD, the phosphorylation of pS202 remains relatively stable with amyloid pathology and disease progression. Notably, there was evidence that in DIAD there is a greater magnitude of phosphorylation and higher levels of t-tau for each category compared with sAD.

Next, we evaluated the proportion of participants in both cohorts who exceeded the values considered abnormal for t-tau and each p-tau isoform for each category of PiB-PET (positive

or negative) and clinical progression (CDR = 0, 0.5 or ≥1). Extended Data Fig. 3 and Supplementary Table 3 show very similar patterns for DIAD and sAD as they relate to the sequential increases in phosphorylation at pT217/T217 and pT181/T181 first, coinciding with the presence of PiB-PET amyloid, followed by increases in pT205/T205 and t-tau with the development and progression of clinical symptoms.

These results indicate that phosphorylation of tau changes at specific sites by disease stage. In DIAN in particular, this suggests a cascade of changes in soluble tau that is more dynamic than was previously realized, and that tau does not monotonically increase in phosphorylation states or rates. The emergence of PiB-PET Aβ and the onset of clinical decline, separated by nearly two decades, mark two important stages of soluble tau phosphorylation changes in DIAD and sAD and suggest that the two different pathways to AD have a similar pattern of evolution in the abnormal processing of tau and expression in the CSF.

Cerebral amyloid pathology is associated with site-specific differences in tau hyperphosphorylation in presymptomatic DIAD

Given the temporal sequence of changes in tau species identified using disease predictability (EYO), we then sought to determine whether changes in other biomarkers across the disease could reveal important associations with the different sites of phosphorylation in DIAD. To explore the relationship of aggregated Aβ and soluble tau phosphorylation, we compared the SUVR value of cortical PiB-PET, which reliably identifies significant brain-aggregated Aß (SUVR > 1.25), with the p-tau isoforms, to determine concordance with aggregated Aß (amyloid-positive SUVR ≥ 1.25; amyloid-negative SUVR < 1.25) (Fig. 3a). pT217/T217 had a 97.2% area under the curve (AUC) (95% confidence interval (CI) = 0.94–0.99); pT181/T181 had an 89.1% AUC (95% CI = 0.83–0.94); pT205/ T205 had a 74.5% AUC (95% CI = 0.69–0.82); t-tau had a 72% AUC (95% CI = 0.65–0.79); and pS202/S202 had a 69% AUC (95% CI = 0.62–0.77) to classify asymptomatic participants as having PiB-PET SUVR levels consistent with aggregated Aβ. This indicates that at the early stages of significant fibrillar Aβ plaques, an increase of phosphorylation has already begun at specific positions linking these two processes in time, and also demonstrates that an increase in the phosphorylation occupancy on T217 could serve as a sensitive diagnostic marker for aggregated Aβ plaque pathology measured by PiB-PET, identifying a potentially unique signature of Aβ-related tau processing in DIAD. When using CSF-soluble Aβ in DIAD to determine abnormal amyloid levels, we found the same order for the soluble tau measures in classifying participants as amyloid positive (Aβ 42/40 ≥ 0.0776) or amyloid negative (Aβ 42/40 < 0.0776), but lower AUC values for each (Supplementary Table 4). Additionally, we compared this mass spectrometry-based method with one of the most advanced immunoassays (the Roche Elecsys pT181 and t-tau CSF electrochemiluminescence method) and found the mass spectrometry method to be superior, indicating a greater sensitivity to detecting early AD pathology in DIAD (Supplementary Table 5).

We then compared the ratios (standardized to a *z* score across all mutation carriers) at four phosphorylation sites and t-tau levels by PiB-PET SUVR quartiles to explore the cross-sectional relationship between total aggregated Aβ load and phosphorylation (Fig. 3b). All

phosphorylation sites except S202 demonstrated increased levels of phosphorylation with greater PiB-PET SUVR; in contrast, pS202/S202 had a decrease in phosphorylation with increasing PiB-PET SUVRs. These results suggest that the events initially leading to increased tau phosphorylation in AD are probably related to aggregated Aβ pathology, potentially through regulation by distinct kinases and phosphatases that are phosphorylationsite specific[41]. Yet, as aggregated Aβ burden continues to increase, there are differences between the amount of phosphorylation that continues to occur among different p-tau isoforms. Importantly, among mutation non-carriers, the only participants who showed an increase in pT217/T217 were those who were amyloid positive (SUVR > 1.25; $n = 4$).

Next, we assessed whether phosphorylation of tau was associated with the anatomical distribution of cerebral aggregated Aβ pathology by exploring the cross-sectional correlations between the baseline p-tau phosphorylation sites and cortical and subcortical regions of amyloid plaque deposition as measured by PiB-PET SUVR in the asymptomatic mutation carriers (Fig. 3d and Supplementary Table 6). pT217/T217, pT181/T181 and pT205/T205 phosphorylation was positively correlated with PiB-PET SUVR throughout the brain, but pS202/S202 was negatively correlated. In the precuneus—a region of early amyloid plaque deposition[38]—correlations with tau phosphorylation were compared based on the strength of bivariate regression, controlling for age, gender and EYO and adjusted for multiple comparisons. We found an order of correlations from greatest to least of pT217/T217 ($r = 0.53$; s.e.m. = 0.06; $P < 10^{-30}$) > pT205/T205 ($r = 0.37$; s.e.m. = 0.075; $P < 10^{-5}$) > pT181/T181 ($r = 0.35$; s.e.m. = 0.075; $P < 10^{-6}$), with positive correlations with PiB-PET SUVR. In contrast, pS202/S202 had an inverse correlation ($r = -0.46$; s.e.m. = 0.067; $P < 10^{-7}$), suggesting that phosphorylation at this site is reduced with increasing aggregated Aβ pathology. We found a similar rank ordering for nearly all regions of PiB-PET and p-tau isoform correlations and statistically significant differences between the different p-tau measure correlations, most commonly for pT217/T217 having the greatest associations.

Neuroimaging markers of disease progression are associated with site-specific differences in tau hyperphosphorylation in presymptomatic DIAD

In addition to using EYO, disease advancement in DIAD can be estimated using neuroimaging measures that track various components of disease progression (for example, brain atrophy and metabolic decline). These measures have been shown to change at different periods of time before symptom onset in DIAD, with declining cerebral metabolism (measured by ^{18}F fluorodeoxyglucose [FDG]-PET) occurring up to 18 years before symptom onset and brain atrophy (determined by magnetic resonance imaging (MRI)) occurring up to 13 years before symptom onset[38,42–44]. This raises the question of whether these biomarkers are likewise correlated with tau phosphorylation at specific sites. To examine this, we performed bivariate cross-sectional correlations between the phosphorylation sites and t-tau and imaging measurements from 34 cortical and six subcortical brain regions, controlling for sex, age and EYO. We focused the analyses on asymptomatic mutation carriers in order to identify any associations at the earliest stages of disease progression, before severe neurodegeneration. The phosphorylation state of pS202/S202 was not included in these analyses given its relative lack of change over disease progression.

MRI

Hyperphosphorylation was inversely associated with cortical thickness in asymptomatic mutation carriers: pT205/T205, and to a lesser extent pT217/T217, was most strongly associated with a decrease in cortical and subcortical thickness throughout the brain (Fig. 4a and Supplementary Table 7), while t-tau levels showed fewer regional associations and weaker correlations. Hyperphosphorylation at pT181/T181 had the lowest overall correlation with cortical atrophy and was restricted to the medial and lateral parietal lobes and medial dorsomedial frontal lobes. This suggests that the initial rise in pT205/T205 at −13 EYO may be related to the underlying process of cortical atrophy, which we have previously shown to begin at approximately −13 EYO in the precuneus[38]. Previous work in DIAN and other DIAD cohorts has shown that significant atrophy, as measured by MRI, does not occur until closer to disease onset, which would indicate that although an increase in CSF tau and phosphorylated tau may in part be related to a passive release in neurodegeneration, their initial rise is probably the consequence of other processes.

FDG-PET

In addition to cortical atrophy, a decline in glucose metabolism in neurons and glia is associated with disease progression in AD. Therefore, we tested whether there were distinct associations between cortical or subcortical metabolic impairment and tau phosphorylation. In the asymptomatic mutation carriers, phosphorylation at pT205/T205 was correlated with glucose hypometabolism throughout the cortex and subcortical regions, as measured by FDG-PET (Fig. 4b and Supplementary Table 8). There were minimal associations identified for the other p-tau sites and t-tau levels in asymptomatic mutation carriers.

Together, these results indicate that the underlying processes leading to neuronal impairment and neurodegeneration during asymptomatic disease progression, as measured by neuroimaging, have different associations with tau phosphorylation, with pT205/T205 most strongly correlated with both.

Cognitive decline and brain atrophy are associated with site-specific differences in tau hyperphosphorylation in DIAD

Previous studies have shown that AD dementia is more closely related to neocortical NFT pathology than neocortical Aβ pathology[45], yet the relationship between soluble tau and cognition remains uncertain[46]. Therefore, we assessed the longitudinal change in the soluble tau phosphorylation ratio and t-tau levels over time compared with clinical outcomes[47]. We performed a mixed-effects model with longitudinal cognitive performance on the neuropsychological composite as the outcome and annual change in CSF tau measures (derived from individual linear mixed-effects (LME) models), time and their interactions as the predictors, adjusting for age, sex, education and familial relation (participants of the same family). We tested all mutation carriers (symptomatic and asymptomatic) for this analysis, in order to include a stage of the disease with significant cognitive decline, and found differential effects between phosphorylation site and cognitive decline. t-tau monotonically increased with worsening cognition and pT217/T217 and pT181/T181 decreased with worsening cognition, while pT205/T205 demonstrated less change relative to cognitive decline and pS202/S202 had no association with cognitive change. As pT217/T217

and pT181/T181 decreased, cognitive decline accelerated (t-value = 2.35, P = 0.02 and 2.11, P = 0.04 (Fig. 5 and Supplementary Table 9). For asymptomatic participants (CDR = 0), there was evidence that an increase in pT181/T181, pT205/T205 and t-tau levels was associated with the initial decline in cognition. This suggests that decreased phosphorylation of T217 and T181, as much as increased soluble t-tau, presents an important marker of cognitive decline. We also evaluated the longitudinal change in the soluble tau phosphorylation ratio and t-tau levels over time compared with longitudinal MRI measures of neurodegeneration (atrophy of the hippocampus and precuneus cortex) and found very similar results to those for cognition (Extended Data Figs. 4 and 5). This further supports the finding that a decrease in the rate of phosphorylation of certain sites of tau represents an important marker of neurodegeneration and symptomatic disease progression.

These findings provide a modification to the current theory that a continuous rise in CSF tau phosphorylation is associated with cognitive dysfunction. We identified two general patterns: for some sites, phosphorylation decreased significantly as cognitive decline began, whereas other sites showed a continuous increase or no change with disease progression (see the increasing versus decreasing rates in Fig. 5).

Increasing levels of t-tau are correlated with baseline cortical NFTs, as measured by tau-PET in DIAD

Recent tau-PET (^{18}F-flortaucipir (AV-1451)) studies with DIAD participants have suggested that an aggregated tau increase occurs following the onset of clinical symptoms[21,25]. We tested the hypothesis that soluble p-tau is a marker of NFT pathology. We explored the relationship between longitudinal changes in CSF t-tau and p-tau isoforms leading up to the time when tau-PET was performed to assess whether faster changes of phosphorylation ratios are associated with higher tau-PET SUVR (greater aggregated tau). In a limited number of participants (ten mutation carriers and four non-carriers), a single tau-PET scan was performed within 72 h of the CSF sample being obtained. For these individuals, CSF samples had also been obtained on previous visits (within 1–3 years).

First, we confirmed that tau-PET SUVR in mutation carriers only increased near the time of symptom onset (Extended Data Fig. 6), suggesting that in DIAD mutation carriers, clinical decline begins when the tau-PET signal starts to increase. Second, we found that a longitudinal increase in CSF t-tau leading up to the time of tau-PET was associated with an elevated global cortical tau-PET composite (P= 0.05) value (Supplementary Table 10) and that this association was related to multiple posterior and limbic cortical regions. Similarly, when exploring the Spearman correlation for the rate of change of soluble tau measures and baseline tau-PET SUVR, we found evidence that increasing levels of t-tau (r = 0.58; P = 0.08) but also pT205/T205 (r = 0.74; P = 0.02) were associated with higher tau-PET levels, whereas there was a suggestion of decreases in pT217/T217 (r = −0.2; P = 0.58) and pT181/T181 (r = −0.27; P = 0.46) with higher tau-PET levels (Extended Data Fig. 7 and Supplementary Table 11). Given the small number of participants available for this analysis, there are limits to the interpretation of these results. However, by measuring multiple sites of phosphorylation simultaneously, these preliminary findings illustrate that the increases in soluble phosphorylated tau identified in DIAD, and presumably in sAD, are not necessarily

a reflection of increases in aggregated tau as measured by tau-PET. In contrast, these results might suggest that a reduction in the phosphorylation rate of some sites (for example, pT181 and pT217) when aggregated tau is increasing could represent a process of sequestration by hyperphosphorylated aggregates[48].

Discussion

Although aggregated tau is a hallmark of AD pathology, important gaps remain in our understanding of how phosphorylation leads to the development of NFTs[2] and neurodegeneration in humans. Here, we demonstrate how patterns of tau phosphorylation in the CSF of DIAD mutation carriers vary over the course of AD progression. We add to the existing clinical literature the demonstration that in DIAD the process of tau phosphorylation and release into the CSF is a dynamic process that: (1) begins once aggregated Aβ pathology (as measured by PiB-PET) is established decades before symptoms, and subsequently unfolds over a period of nearly two decades; (2) occurs in a pattern such that phosphorylation of different tau sites closely follows disease progression, as revealed by levels of other biomarkers; and (3) decreases significantly in a site-dependent manner near the onset of cognitive decline and the rise in aggregated tau (as measured by tau-PET). Together, these results indicate that this method of quantifying soluble tau phosphorylation occupancy can track the AD process across its preclinical to symptomatic stages, providing a signature of p-tau pathology for this disease (Supplementary Table 12). Moreover, they challenge the purported roles of tau/p-tau in DIAD, and possibly AD in general, and recapitulate in humans those findings from animal studies that link Aβ pathology to tau hyperphosphorylation[32,34,36,49] and active cellular release, rather than release of dying neurons.

Although causality needs to be addressed in future studies, the contemporaneous increases in pT217/T217, pT181/T181 and PiB-PET SUVR suggest that the phosphorylation of tau in AD is closely linked to Aβ pathology. This is consistent with recent work in AD transgenic mice[31,32,34,50,51] and in humans, which demonstrates that tau and hyperphosphorylated tau are released from cells in an active process that is increased in the presence of aggregated Aβ[33]. Our results link Aβ pathology to a distinct change in soluble tau levels and phosphorylation patterns, shedding light on the phenomenon in which significant elevation of p-tau occurs in AD but not in other neurodegenerative tauopathies[17,18].

Recent work has shown that an increase and spread of neuritic tau aggregates (paired helical filaments in dystrophic neurites) in Aβ transgenic mice is enhanced by the presence of aggregated Aβ, occurring before established somatic NFTs[31]. It is possible that the very early increase we find in pT217/T217 and pT181/T181 may reflect this ‘early’ tau response to aggregated Aβ and might explain the global association of PiB-PET SUVR with these isoforms that we identified. Additionally, the lack of clinical symptoms seen during this early elevation in phosphorylation of tau suggests it occurs years before the onset of significant neurodegeneration. Our findings of an increase in pT205/T205 being associated with a decline in synaptic homeostasis could represent a protective process resulting in increased phosphorylation at T205 with synaptic distress from chronic Aß exposure, at least in DIAD[51]. Importantly, we have shown that t-tau levels appear to rise to similar levels with

disease progression (Supplementary Fig. 2). This would indicate that the differences we have detected in the phosphorylation occupancy in DIAD are less likely to just reflect a difference in the amount of intraneuronal tau protein produced and released into the CSF compartment. Rather, it might suggest that with different stages of the disease (Fig. 1), there are unique activations of the different kinases responsible for phosphorylating the tau protein preferentially at specific sites[41].

These data call into question some common assumptions about the role of soluble tau and p-tau in AD. Specifically, the current diagnostic framework in AD emphasizes the presence of biomarkers representing AD-specific and non-specific pathologies (for example, Aβ, p-tau and tau)[15]. Within this diagnostic framework, soluble p-tau and t-tau are often presumed to be passively released from degenerating neurons, with p-tau associated with aggregated NFTs and t-tau associated with axonal degeneration. Cross-sectional associations between phosphorylation levels and tau-PET measures in previous studies and our own data (Extended Data Fig. 8 and Supplementary Table 13) suggest that soluble p-tau and aggregated tau by tau-PET are correlated. In contrast, the more appropriate longitudinal measures indicate that soluble tau phosphorylation occupancy decreases during the time of tau increase[25], at least in DIAD, demonstrating an inverse correlation. One possible explanation for this is similar to what has been observed with soluble/aggregated Aβ[52]: that the dramatic increase of aggregated tau sequesters phosphorylated tau[53] in the brain, decreasing CSF levels. In addition, early phosphorylation modifications suggest that hyperphosphorylation, although a marker of pathophysiology, is not necessarily a marker of tau-related NFTs.

A reduction of tau through proteostatic mechanisms cannot be excluded[54] as a cause for the decrease in phosphorylation, but the continued increase of t-tau (Supplementary Fig. 3) would suggest that this is probably not the cause for the decreasing rate of phosphorylation for some sites. Similarly, a recent study has shown that the new production of tau and levels in the CSF do not appear to change in the presence of elevated tau (tau-PET)[33]. In either case, our findings of the negative correlation between the phosphorylation ratios of pT217/T271 or pT181/T181 and longitudinal cognitive decline and MRI measures of neurodegeneration highlight the importance of the reversal in phosphorylation rate of some tau sites in disease progression. Elucidating the cause for this decline could lead to a better understanding of the links between soluble tau and neuronal dysfunction and the use of CSF p-tau/tau in AD prognostication.

In summary, we have demonstrated that in AD associated with autosomal dominant mutations, CSF tau hyperphosphorylation occurs very early and exhibits pattern of site-specific changes at different stages of the disease. The underlying mechanisms behind these findings will have important implications for the understanding of the disease and for tau-directed therapies for AD.

Methods

Study design

Participants with at least a 50% risk of inheriting a DIAD mutation from families with a confirmed genetic mutation in *PSEN1*, *PSEN2* or *APP* were enrolled in the DIAN study (National Institute on Aging U19 Clinical Trial; AG032438) (dian.wustl.edu; clinicaltrials.gov number NCT00869817)[55]. All procedures were approved by the Institutional Review Board (IRB) of Washington University and conformed to local IRB and ethics committee guidelines. The presence or absence of a DIAD mutation was determined using PCR-based amplification of the appropriate exon, followed by Sanger sequencing. At each study visit, participants underwent comprehensive clinical assessments, cognitive testing, neuroimaging and CSF studies; however, at each visit, each participant may not have completed all of these study procedures. The details of study structure and assessments can be found in previous publications[9,55]. Follow-up intervals were determined by the clinical status (normal or impaired) of each participant and by their EYO, and ranged from annual to every 3 years. Data were obtained from quality-controlled data (annual quality assessments for irregular results and missing data from 26 January 2009 to 30 June 2017) and included 370 participants (n = 150 with longitudinal CSF evaluations, with a median time between visits of 2.8 years).

The non-familial population represented two cohorts recruited at the Knight Alzheimer Disease Research Center at Washington University and the Centres Memoire Resources et de Recherche, Centre Hospitalier Universitaire (CHU) de Montpellier. All participants underwent detailed clinical cognitive assessments, CSF assessments and a diagnosis of preclinical AD or AD confirmed with abnormal amyloid biomarkers. All procedures were approved by the IRB of Washington University and ethics committees at CHU de Montpellier.

EYO

In DIAD, there is almost 100% penetrance, with age at symptom onset in mutation carriers being relatively consistent for each mutation and within each family. This allows for the designation of EYO. EYO was defined as follows. A parental age at earliest symptom onset was established for each participant by semi-structured interview. The parental age at onset for each mutation was then entered into a database consisting of the combined symptom onset values from DIAN and those from previous publications on DIAD cohorts. These were used to compute an average age of onset specific to each mutation[39]. The mutation-specific age of onset was subtracted from each participant's age at the time of clinical assessment to define the individual's EYO. When a specific mutation's average age of onset was unknown, the parental or proxy age of onset was used to define the EYO[39]. For participants who were symptomatic at baseline, as assessed by a CDR > 0, the reported age of actual symptom onset was subtracted from the age at each clinical assessment to define EYO.

Clinical assessments

Standardized clinical evaluations, including the use of a study partner, were performed for each DIAD participant. The CDR was used to indicate dementia stage. Participants were

rated as cognitively normal (CDR = 0) or having very mild dementia (CDR = 0.5), mild dementia (CDR = 1) or moderate dementia (CDR = 2)[40]. Evaluating clinicians were blind to genetic status. A comprehensive neuropsychological battery assessing general cognitive function, memory, attention, executive function, visuospatial function and language was performed at each visit[56]. From these tests, we developed a cognitive composite that reliably detects decline across the range of EYO and CDR values[57]. The composite represents the average of the *z* scores from tests including episodic memory, complex attention and processing speed and a general cognitive screen (mini-mental state examination).

For the non-familial cohorts, all participants underwent a standardized, detailed clinical assessment specific to each of the two centers. A diagnosis of AD was based on the National Institute of Neurological and Communicative Disorders and Stroke-Alzheimer Disease and Related Disorders Association[58] criteria, and was confirmed with abnormal amyloid biomarkers. Dementia severity was based on the CDR. Additional details of the cohort can be found in previous publications[59].

CSF tau analyses

CSF was collected, via standard lumbar puncture procedures using an atraumatic Sprotte spinal needle (22 Ga), into two 13-ml polypropylene tubes. CSF was flash-frozen upright on dry ice. Samples collected in the United States were shipped overnight on dry ice to the DIAN Biomarker Core laboratory at Washington University (St. Louis, Missouri, United States), whereas samples collected at international sites were stored at −80 °C and shipped quarterly on dry ice. Upon arrival, each sample was subsequently thawed, combined into a single polypropylene tube and aliquoted (500 µl each) into polypropylene microcentrifuge tubes (05–538-69C; Corning Life Science), after which they were re-flash-frozen on dry ice and stored at −80 °C.

Each thawed CSF sample was mixed with 25 µl of a solution containing ^{15}N-441 tau internal standard (2.5 ng per sample), 50 mM guanidine, 10% NP-40 and 10× protease inhibitor cocktail (Roche). Tau was extracted by immune capture using incubation under rotation at room temperature for 2 h with 20 µl of sepharose beads cross-linked to Tau-1 (tau epitope 192–199) and HJ8.5 (tau epitope 27–35) antibodies. Beads were spun by centrifugation, then rinsed three times with 1 ml of 25 mM triethylammonium bicarbonate. Samples were digested overnight at 37 °C with 400 ng of trypsin Gold (Promega). AQUA peptides (Life Technologies) were spiked to obtain an amount of 5 fmol per labeled phosphorylated peptide and 50 fmol per labeled unmodified peptide in each sample. The peptide mixture was loaded on TopTip C18 tips, washed with 0.1% formic acid solution and eluted with 60% acetonitrile/0.1% formic acid solution. Eluates were dried using a Speedvac and dried samples were stored at −80 °C before analysis. Samples were resuspended in 25 µl of 2% acetonitrile/0.1% formic acid. Extracts were analyzed by nano liquid chromatography coupled to high-resolution tandem mass spectrometry (HRMS/MS) using parallel reaction monitoring using HCD fragmentation. Nano liquid chromatography-HRMS/MS experiments were performed using a nanoAcquity UPLC system (Waters) coupled to a Fusion Tribrid mass spectrometer (Thermo Fisher Scientific). For each sample, 5 µl was injected. Peptide separation was achieved at 60 °C in 24 min on a Waters HSS T3 column (75 µm × 100 mm;

1.8 μm). Mobile phases were: (A) 0.1% formic acid in water; and (B) 0.1% formic acid in acetonitrile. The gradient used was 0.5% B at 0 min, 5% B at 7.5 min and 18% B at 22 min, then the column was rinsed for 2 min with 95% B. The flow rate was set at 700 nl min^{-1} for 7.5 min, then 400 nl min^{-1} for the rest of the analysis. Data were acquired in the positive ion mode at a spray voltage of 2,200 V (Nanospray Flex ion source; Thermo Fisher Scientific) and the ion transfer tube was set at 270 °C. The S-lens radio frequency voltage was set at 60 V. HRMS/MS transitions (Supplementary Table 14) were extracted using Skyline software (MacCoss laboratory). CSF tau phosphorylation levels were calculated using measured ratios between HRMS/MS transitions of endogenous unphosphorylated peptides and ^{15}N-labeled peptides from the protein internal standard. Ratios of phosphorylation on T181, S202, T205 and T217 were measured using the ratio of the HRMS/MS transitions from phosphorylated peptides and the corresponding unphosphorylated peptides. Each phosphorylated/unphosphorylated peptide endogenous ratio was normalized using the ratio measured on the HRMS/MS transitions of the corresponding AQUA phosphorylated/unphosphorylated peptide internal standards.

All samples from the DIAN longitudinal and the cross-sectional studies were run together with waste CSF (longitudinal and cross-sectional study) and CSF pool (cross-sectional study) quality controls to monitor inter-assay variability for each variable at low CSF tau (normal level) and high CSF tau levels (AD typical level). The corresponding values and inter-assay coefficient of variation are incorporated in Supplementary Tables 1–5. In both studies, the inter-assay coefficient of variation was typically below 20%. A low percentage of the investigated samples had CSF pT205 and pT217 levels below the lowest limit of quantitation (4.7 and 4.5%, respectively), defined as levels providing liquid chromatography–mass spectrometry signals leading to a coefficient of variation of more than 20%.

CSF samples from sAD at Washington University were collected as described previously[59]. Aliquots from the collection performed at hour 32 were used for the analysis. CSF samples from sAD at Montpellier were collected in polypropylene tubes using lumbar puncture methods (Starstedt; 10 ml; 62.610.201) in line with standard operating procedures[60], transferred at a temperature of 4 °C within less than 4 h to the laboratory and centrifuged at 1,000*g* at 4 °C for 10 min. Aliquots of CSF supernatant (0.5 ml) were subsequently collected in 1.5-ml Eppendorf microtubes (Eppendorf Protein LoBind; ref0030108.116) and stored at −80 °C before shipping on dry ice, additional storage at −80 °C and analysis. These samples were used and tested without performing an additional freeze–thaw cycle. The methods used for the handling and traceability of the samples were in keeping with the procedures recommended in the biobank quality standard NFS 96–900, for which the laboratory is certified. Additional details were described previously[61].

Brain imaging

Amyloid deposition, glucose metabolism, tau (NFT)-PET and cortical thickness/subcortical volumes were assessed using ^{11}C-PiB-PET, ^{18}F-FDG-PET, ^{18}F-AV-1451 and volumetric T1-weighted MRI scans, respectively. Standard procedures were used to ensure consistency in the data collection of all DIAN sites[38]. The ^{11}C-PiB-PET scan consisted of 70 min of

dynamic scanning after a bolus injection of ~13 mCi of PiB with regional standard uptake ratios (SUVRs) determined from the 40- to 70-min timeframe. The ^{18}F-FDG-PET scan started 30 min after a bolus injection of ~5 mCi and lasted 30 min. The ^{18}F-AV-1451 data were acquired from the 80- to 100-min window after bolus injection and were converted to SUVRs. The T1 magnetic resonance sequence was an accelerated magnetization-prepared rapid acquisition with gradient echo acquired on 3T scanners (parameters: repetition time = 23,000; echo time = 2.95; 1.0 × 1.0 × 1.2 mm^3 resolution). All tau and PiB-PET data have been reported in previous publications[8,21].

The PiB and FDG SUVRs from 34 cortical and six subcortical regions of interest (ROIs) were obtained using FreeSurfer software (http://surfer.nmr.mgh.harvard.edu/). The SUVRs were processed with total cerebellum gray matter as reference regions and ROI data were corrected for partial volume effects using a regional point spread function[62] in a geometric transfer matrix framework.

Statistical analysis

Baseline characteristics of the participants were summarized as means ± s.d. for continuous variables and *n* (column percentage) for categorical variables. *P* values for comparing the differences among asymptomatic mutation carriers, symptomatic mutation carriers and non-carriers, as defined at baseline, were obtained using LME models for continuous variables and generalized LMEs with a logistic link for categorical variables. All of the models incorporated a random family effect to account for the correlations on the outcome measures between participants within the same family. The cut point for baseline cortical PiB-PET SUVR was chosen such that the difference in the longitudinal rate of change of cortical PiB-PET between mutation carriers and non-carriers first starts to differ significantly from 0.

The cross-sectional relationships of the different tau phosphorylation sites with PiB, FDG and cortical thickness/subcortical volume were evaluated in all asymptomatic mutation carriers (CDR = 0; $n = 152$) using multivariate LME models on each ROI. The models included fixed effects of EYO and random intercepts at the family level. Compared with the simple correlation estimation method (Pearson or Spearman correlation), the multivariate LME model can adjust for covariates such as EYO, as well as accounting for the correlation within the family cluster[63,64]. *P* values for testing the correlations were corrected using the Benjamini–Hochberg method[65], to control the false discovery rate due to multiple testing.

For the within-individual annual rate of change over the longitudinal follow-up, the best linear unbiased predictors for each biomarker were estimated using LME models, which were then plotted against the baseline EYO to examine biomarker trajectories. LME or linear spline mixed-effects models, where appropriate, were then used to determine the baseline EYO point from which mutation carriers became significantly different from non-carriers in the baseline level and the rate of change for each biomarker. The details of the linear spline mixed-effects models can be found in a recent publication[8]. The LME or linear spline mixed-effects models included the fixed effects of mutation group (mutation carrier or non-carrier), baseline EYO, time since baseline and all possible two- or three-way interactions among them. Sex, years of education and apolipoprotein-E $\varepsilon 4$ status were considered as covariates, but only those effects that were significant were retained in the

models. The random effects included in the models were the random intercepts for family clusters, individual random intercept and random slope with unstructured covariance matrix, to account for the within-subject correlation due to repeated measures. The adjusted difference in the mean level at baseline and difference in the rates of change between mutation carriers and non-carriers were then tested using the approximate *t*-test derived from the models to determine the first EYO point at which the difference became significant.

To visualize the differences in the rates of change among t-tau, tau phosphorylation site, cortical PiB and global cognition across the range of EYO values, measures of mutation carriers were first standardized using the mean and standard deviation of non-carriers. The rate of change of each measure for each mutation carrier was then calculated using LME modeling, and LOESS curves were fitted to visually represent the trajectories of the standardized rates of change over the EYO.

The utility of the baseline and annual rate of change of t-tau and p-tau in predicting longitudinal cognitive decline among mutation carriers was evaluated using LME modeling, controlling for the effect of baseline age, sex and apolipoprotein-E *ε*4 status. Random effects in the models included the random intercepts for family clusters, individual random intercept and random slope with unstructured covariance matrix.

Linear regressions were used to examine whether the annual rate of change of tau and p-tau position for mutation carriers and non-carriers, leading up to and including the point when the tau-PET was performed, could predict tau-PET SUVR, controlling for the effect of age. Due to the limited number of participants, a family cluster was not included.

All analyses were conducted using SAS 9.4 (SAS Institute) and RStudio (version 3.4.3). $P < 0.05$ was considered to be statistically significant and all statistical tests were two sided.

Extended Data

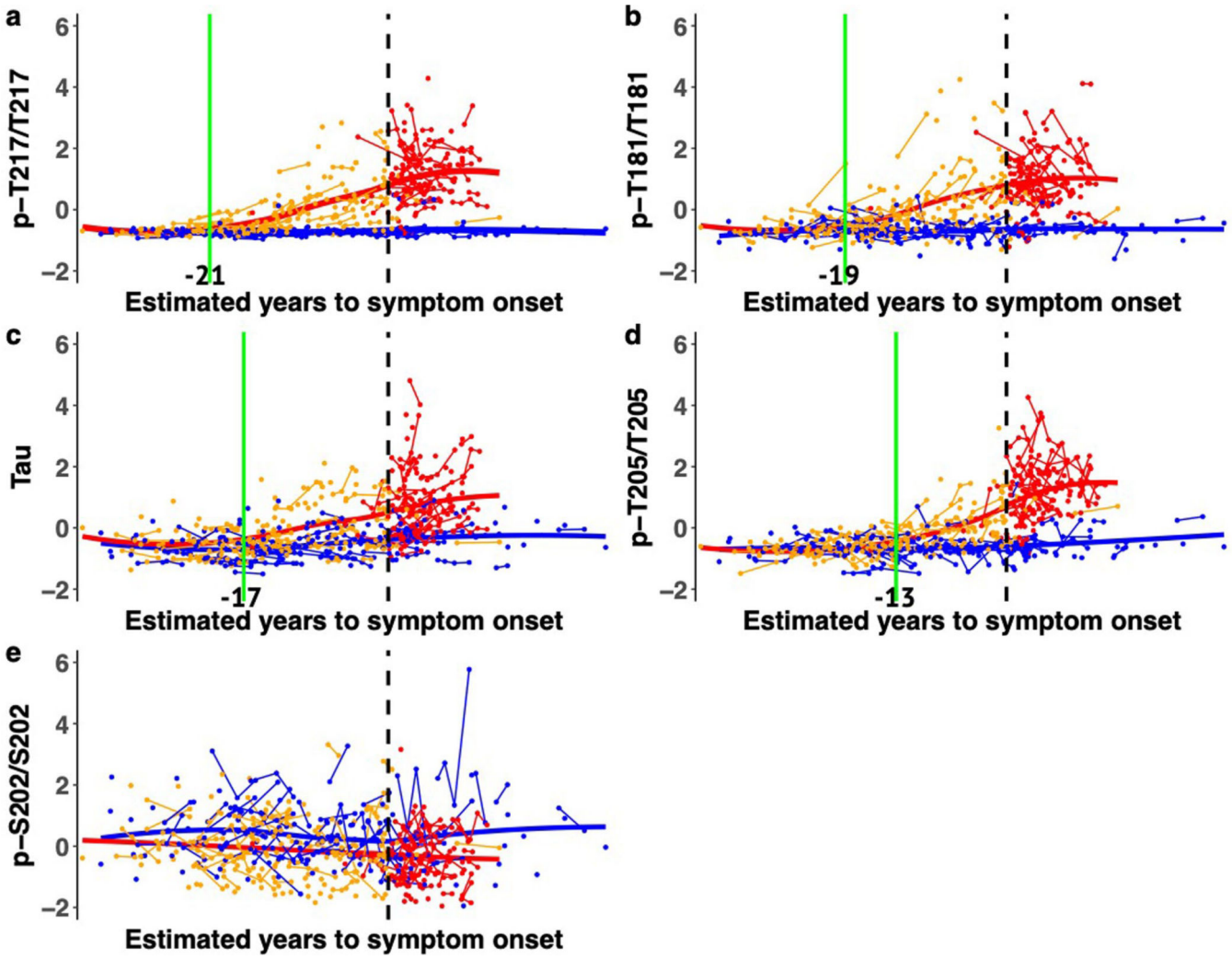

Extended Data Fig. 1 |. Individual longitudinal changes of different phosphorylated-tau sites and total tau highlights differences in the time of increase relative to disease onset.

Individual, z-transformed, longitudinal changes in the ratio of phosphorylation of **a**, pT217/T217, **b**, pT181/T181 **c**, total tau, **d**, pT205/T205, and **e**, pS202/S202 for mutation carriers (orange = asymptomatic mutation carriers, (n = 152), red = symptomatic mutation carriers (n = 77)) and non-carriers (blue, (n = 141)) across the estimated years to symptom onset (EYO). The vertical dashed line is the point of expected symptom onset, the vertical green line represents the model estimated time when the rate of change for each p-tau isoform becomes greater for mutation carriers compared to non-carriers.

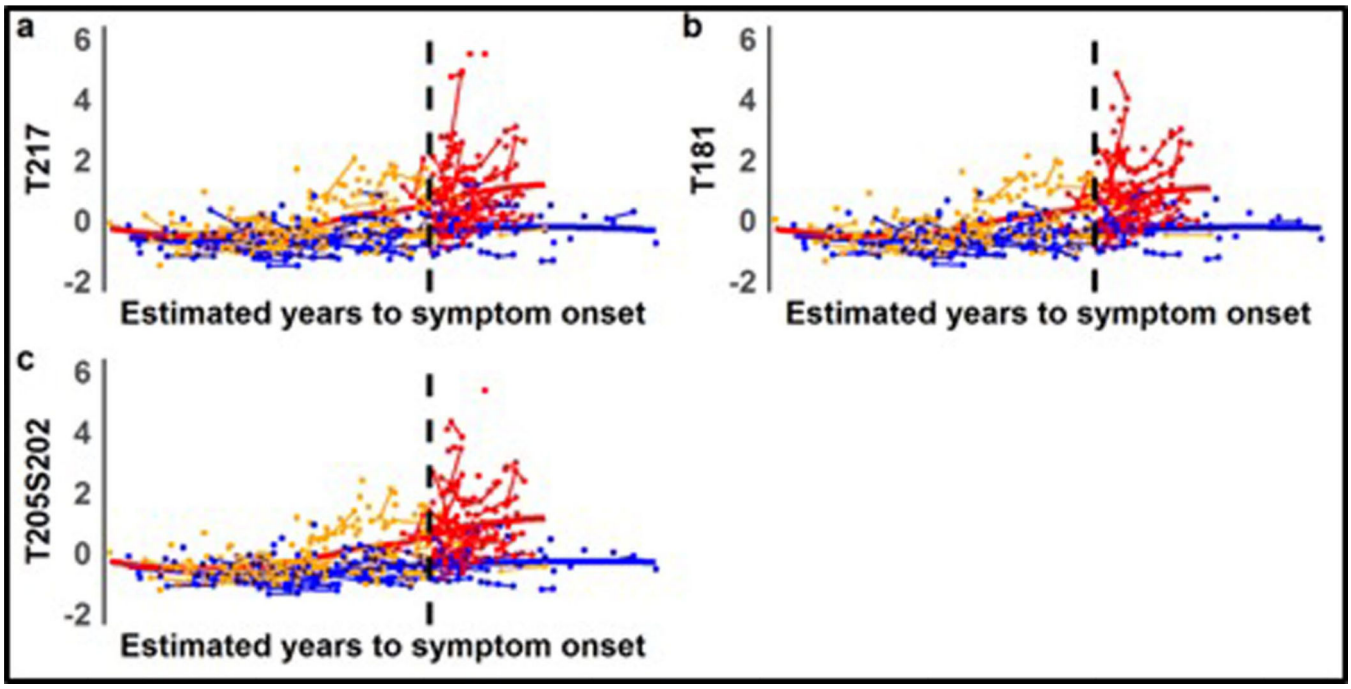

Extended Data Fig. 2 |. Individual longitudinal changes of different unphosphorylated-tau sites. Individual, z-transformed, longitudinal changes in the unphosphorylated levels of **a**, T217, **b**, T181 **c**, T205 for mutation carriers (orange = asymptomatic mutation carriers, (n = 152), red = symptomatic mutation carriers (n = 77)) and non-carriers (blue, (n = 141)) across the estimated years to symptom onset (EYO). The solid line represents a LOESS fit to cross-sectional and longitudinal data. The vertical dashed line is the point of expected symptom onset. Compared to the phosphorylation ratios of each site (Extended Data Fig. 1), the increase in the unphosphorylated levels appears to be more similar over the progression of disease.

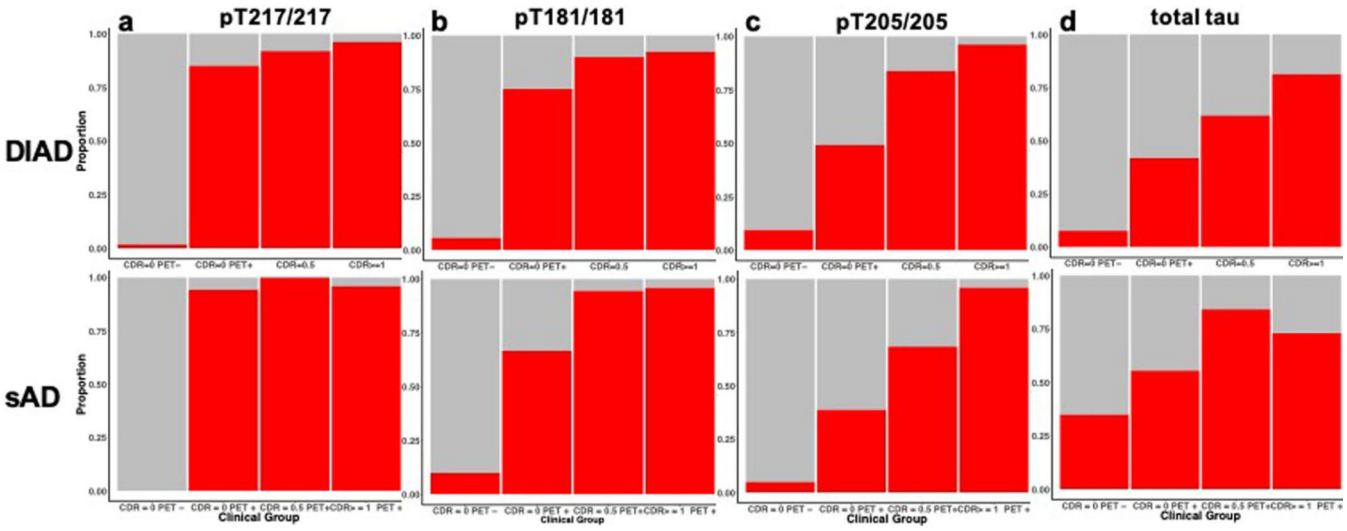

Extended Data Fig. 3 |. Change in tau phosphorylation state is site dependent and related to amyloid PET and disease stage in DIAD and sAD.

Bar charts illustrating the proportion of participants that have p-tau ratios and total tau levels that exceed the normal values (biomarker + (red)) (a- d) as the stage of disease progresses from cognitively normal/PiB-PET normal to cognitively normal/PiB-PET positive then to mild dementia (CDR 0.5) and greater (CDR >0.5). The top row is DIAD (n = 210) and the bottom row sAD (n = 83). The figure demonstrates very similar patterns for each phosphorylation ratio and total tau levels across the progression of disease and indicate a similar ordering in DIAD and SAD, generalizing these findings to AD.

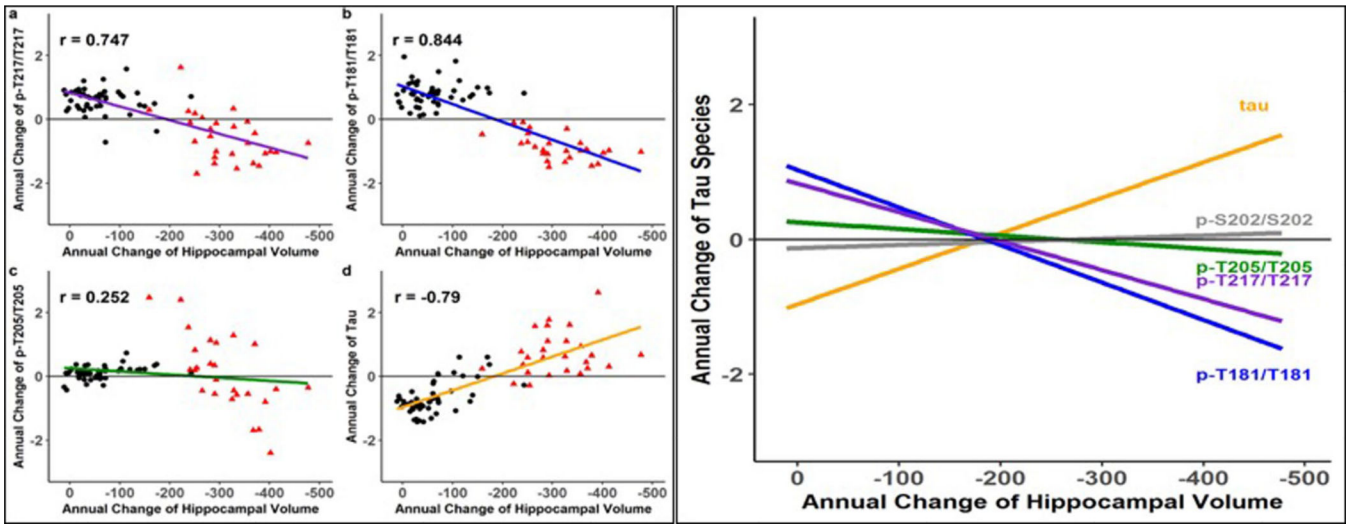

Extended Data Fig. 4 |. Elevated levels of tau phosphorylation decline in some sites with atrophy of hippocampal volumes in contrast to a continued rise in total tau.

Estimated individual annual rates of change of p-tau isoforms and total tau, standardized by the mean and standard deviation of the estimated rate of change for all mutation carriers, (y-axis) for mutation carriers were correlated with the annual change in hippocampal volumes (**a-d**). The linear regression was fit to those with no dementia (CDR 0, black circle, n = 48) and dementia (CDR > 0, red triangle, n = 27). A decline in pT217/T217 (a), r = 0.74($p < 0.0001$), pT181/T181 (b), r = 0.84 ($p < 0.0001$) and pT205/T205, r = 0.25 (p = 0.03) phosphorylation rate was associated with hippocampal volume decline. For total tau there was an inverse correlation with atrophy (d), r = −0.79($p < 0.0001$). (e) A linear fit for all mutation carriers demonstrates there are distinct associations between declining cognition and changes in the different p-tau isoforms and total tau: with decreases in pT217/T217 and pT181/T181 and an increase in total tau associated with cognitive decline; and no associations with pT205/T205 or pS202/S202. This suggests that soluble tau species are not equivalent in AD (pS202/S202) is shown here to demonstrate the lack of association with cognition, r = −0.07 (p = 0.57). Statistical significance of the correlations was calculated using z test.

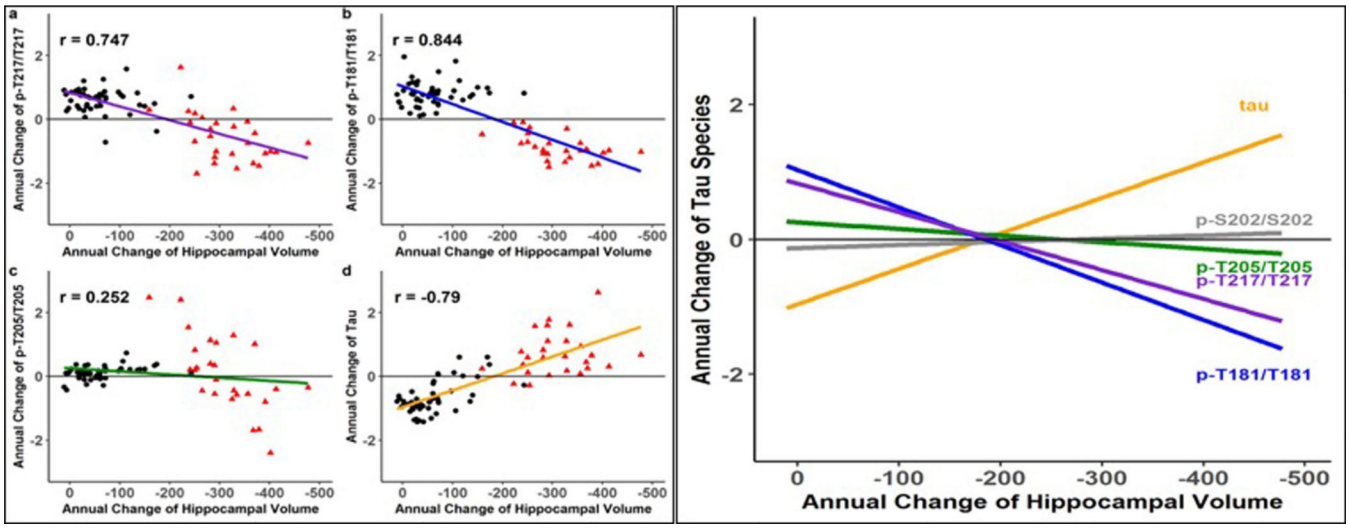

Extended Data Fig. 5 |. Elevated levels of tau phosphorylation decline in some sites with atrophy of precuneus cortex in contrast to a continued rise in total tau.

Estimated individual annual rates of change of p-tau isoforms and total tau, standardized by the mean and standard deviation of the estimated rate of change for all mutation carriers, (y-axis) for mutation carriers were correlated with the annual change in hippocampal volumes (**a-d**). The linear regression was fit to those with no dementia (CDR 0, black circle, n = 48) and dementia (CDR > 0, red triangle, n = 27). A decline in pT217/T217 (a), r = 0.75 ($p <$ 0.0001), pT181/T181 (b), r = 0.83 ($p < 0.0001$) and pT205/T205, r = 0.19 ($p = 0.09$) phosphorylation rate was associated with precuneus cortical decline. For total tau there was an inverse correlation with atrophy (d), r = −0.77($p < 0.0001$). (e) A linear fit for all mutation carriers demonstrates there are distinct associations between declining cognition and changes in the different p-tau isoforms and total tau: with decreases in p-T217 and p-T181 and an increase in total tau associated with cognitive decline; and no associations with pT205/T205 or pS202/S202. This suggests that soluble tau species are not equivalent in AD (pS202/S202 is shown here to demonstrate the lack of association with cognition, r = −0.04 ($p = 0.72$). Statistical significance of the correlations was calculated using two-sided *t* tests.

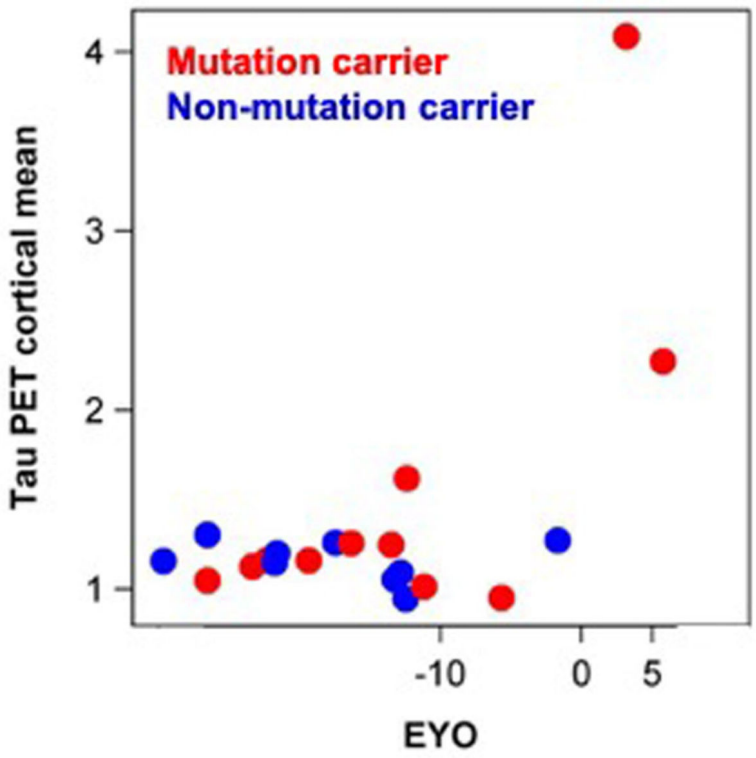

Extended Data Fig. 6 |. Tau PET increases near symptom onset in DIAD mutation carriers.
The mean cortical standardized unit value ratio (SUVR), y-axis, for mutation carriers (red, n = 12) and non-carriers (blue, n = 9) over estimated years to symptom onset (EYO), x-axis, for those participants with a longitudinal CSF evaluation preceding the time of tau-PET. The plot shows that for mutation carriers there is little elevation in tau-PET until the point of estimated symptom onset (EYO=0). This figure shows that the neurofibrillary tangle (NFT) pathology detected by AV-1451 occurs much later than the increase in multiple soluble phosphotau sites suggesting that these soluble markers of tau are likely a marker of NFT pathology, but rather might predispose to the development of the hyperphosphorylated, insoluble tau deposits characteristic of AD pathology.

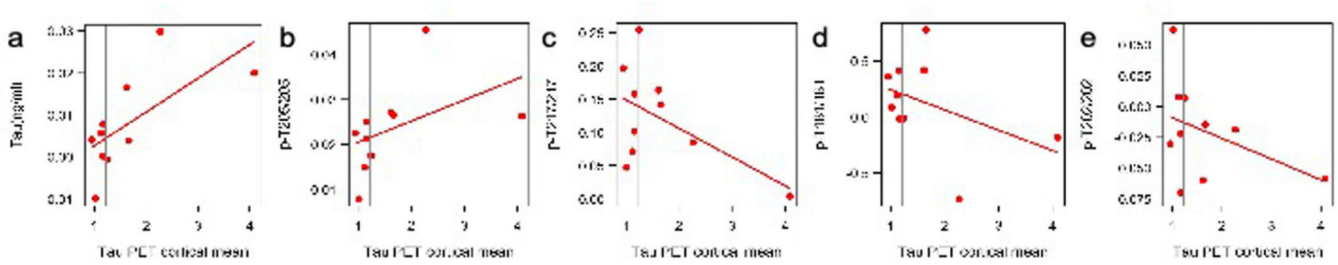

Extended Data Fig. 7 |. Longitudinal change in tau and tau phosphorylation sites are differentially related to neurofibrillary tau (tau-PET) in dominantly inherited AD.

Individual, rates of change of phosphorylation and total tau (y-axis) in mutation carriers only leading up to the time of tau-PET scan (x-axis) (n = 12). The vertical line is an SUVR of 1.22 and represents a conservative estimate of the point when cortical tau-PET is considered elevated for tau aggregates compared to non-carriers. The plots suggest that increases in soluble tau and p-T205 are associated with higher levels of aggregated tau, whereas the rate of phosphorylation at p-T217 and p-T181 decrease as levels of aggregated tau increase. These findings suggest that there are differences between increasing levels of tau and phosphorylation at different sites and may indicate that, in some instances, soluble p-tau maybe sequestered as the burden of hyperphosphorylated aggregates increase with the spreading of tau pathology. They also suggest that with the increase in aggregated tau there is a rise in soluble tau levels which could represent either passive or active release with greater burden of aggregated tau pathology.

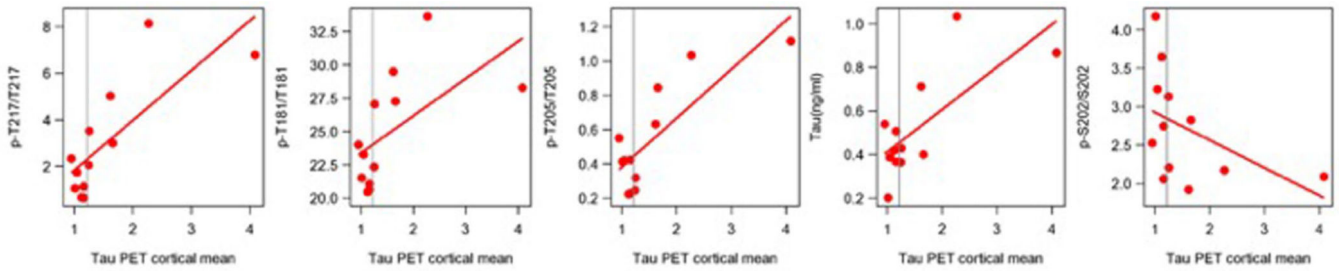

Extended Data Fig. 8 |. Spearman correlation of the cross-sectional association of p-tau phosphorylation, total tau (y-axis) and tau PET (x-axis) for mutation carriers (n = 12).
The vertical line is an SUVR of 1.22 and represents a conservative estimate of the point when cortical tau-PET is considered elevated for tau aggregates compared to non-carriers.

Supplementary Material

Refer to Web version on PubMed Central for supplementary material.

Acknowledgements

Data collection and sharing for this project was supported by the DIAN (UF1AG032438), funded by the National Institute on Aging, German Center for Neurodegenerative Diseases and Raul Carrea Institute for Neurological Research (FLENI), with partial support via research and development grants for dementia from the Japan Agency for Medical Research and Development and the Korea Health Technology R&D Project, through the Korea Health Industry Development Institute, MRC Dementias Platform UK (MR/L023784/1 and MR/009076/1) and AOI Lady Biobank CHU. The development and performance of the mass spectrometry analyses was supported by the Alzheimer's Association Research Fellowship (AARF-16-443265 to N.R.B.), Fondation Plan Alzheimer (to A.G. and S.L.), BrightFocus (A20143845 to R.J.B.), the National Institute of Neurological Disorders and Stroke (R01NS095773 to R.J.B.) and the National Institute on Aging (K23 AG046363 to E.M.). This manuscript has been reviewed by DIAN Study investigators for scientific content and consistency of data interpretation with previous DIAN Study publications. We acknowledge the altruism of the participants and their families and contributions of the DIAN research and support staff at each of the participating sites for their contributions to this study. We thank J. Ringman and B. Ghetti for reviewing the manuscript and making suggestions.

Dominantly Inherited Alzheimer Network

Ricardo Allegri[7], Randy Bateman[31], Jacob Bechara[19], Tammie Benzinger[31], Sarah Berman[32], Courtney Bodge[33], Susan Brandon[31], William (Bill) Brooks[19], Jill Buck[34], Virginia Buckles[31], Sochenda Chea[35], Jasmeer Chhatwal[36,37], Patricio Chrem Mendez[7], Helena Chui[38], Jake Cinco[39], Jack Clifford[35], Carlos Cruchaga[31], Tamara Donahue[31], Jane Douglas[39], Noelia Edigo[7], Nilufer Erekin-Taner[35], Anne Fagan[31], Martin Farlow[34], Colleen Fitzpatrick[36], Gigi Flynn[31], Nick Fox[39], Erin Franklin[31], Hisako Fujii[10], Cortaiga Gant[31], Samantha Gardener[23], Bernardino Ghetti[34], Alison Goate[40], Jill Goldman[41], Brian Gordon[31], Neill Graff-Radford[35], Julia Gray[31], Alexander Groves[31], Jason Hassenstab[31], Laura Hoechst-Swisher[31], David Holtzman[31], Russ Hornbeck[31], Siri Houeland DiBari[25], Takeshi Ikeuchi[9], Snezana Ikonomovic[32], Gina Jerome[31], Mathias Jucker[28], Celeste Karch[31], Kensaku Kasuga[9], Takeshi Kawarabayashi[11], William (Bill) Klunk[32], Robert Koeppe[42], Elke Kuder-Buletta[28], Christoph Laske[28], Jae-Hong Lee[43], Johannes Levin[25], Ralph Martins[23], Neal Scott Mason[44], Colin Masters[22], Denise Maue-Dreyfus[31], Eric McDade[31], Hiroshi Mori[10], John Morris[31], Akem Nagamatsu[11], Katie Neimeyer[41], James Noble[41], Joanne Norton[31], Richard Perrin[31], Marc Raichle[31], Alan Renton[40], John Ringman[38], Jee Hoon Roh[43], Stephen Salloway[33], Peter Schofield[19], Hiroyuki Shimada[10],

Wendy Sigurdson[31], Hamid Sohrabi[23], Paige Sparks[36], Kazushi Suzuki[11], Kevin Taddei[23], Peter Wang[31], Chengjie Xiong[31] and Xiong Xu[31]

[31]St. Louis School of Medicine, Washington University, St. Louis, MO, USA. [32]University of Pittsburgh, Pittsburgh, PA, USA. [33]Butler Hospital, Brown University, Providence, RI, USA. [34]Indiana University, Bloomington, IN, USA. [35]Mayo Clinic Jacksonville, Jacksonville, FL, USA. [36]Brigham and Women's Hospital, Boston, MA, USA. [37]Massachusetts General Hospital, Boston, MA, USA. [38]University of Southern California, Los Angeles, CA, USA. [39]University College London, London, UK. [40]Icahn School of Medicine at Mount Sinai, New York, NY, USA. [41]Columbia University, New York, NY, USA. [42]University of Michigan, Ann Arbor, MI, USA. [43]Asan Medical Center, Seoul, Republic of Korea. [44]University of Pittsburgh Medical Center, Pittsburgh, PA, USA.

References

1. Goedert M, Spillantini MG, Jakes R, Rutherford D & Crowther RA Multiple isoforms of human microtubule-associated protein tau: sequences and localization in neurofibrillary tangles of Alzheimer's disease. Neuron 3, 519–526 (1989). [PubMed: 2484340]
2. Grundke-Iqbal I et al. Abnormal phosphorylation of the microtubule-associated protein τ (tau) in Alzheimer cytoskeletal pathology. Proc. Natl Acad. Sci. USA 83, 4913–4917 (1986). [PubMed: 3088567]
3. Kimura T, Sharma G, Ishiguro K &Hisanaga S Phospho-tau bar code: analysis of phosphoisotypes of tau and its application to tauopathy. Front. Neurosci12, 44 (2018). [PubMed: 29467609]
4. Crowther RA Straight and paired helical filaments in Alzheimer disease have a common structural unit. Proc. Natl Acad. Sci. USA 88, 2288–2292 (1991). [PubMed: 1706519]
5. Fitzpatrick AWP et al. Cryo-EM structures of tau filaments from Alzheimer's disease. Nature 547, 185–190 (2017). [PubMed: 28678775]
6. Price JL, Davis PB, Morris JC & White DL The distribution of tangles, plaques and related immunohistochemical markers in healthy aging and Alzheimer's disease. Neurobiol. Aging 12, 295–312 (1991). [PubMed: 1961359]
7. Qian J, Hyman BT &Betensky RA Neurofibrillary tangle stage and the rate of progression of Alzheimer symptoms: modeling using an autopsy cohort and application to clinical trial design. JAMA Neurol. 74, 540–548 (2017). [PubMed: 28288263]
8. McDade E et al. Longitudinal cognitive and biomarker changes in dominantly inherited Alzheimer disease. Neurology 91, e1295–e1306 (2018). [PubMed: 30217935]
9. Bateman RJ et al. Clinical and biomarker changes in dominantly inherited Alzheimer's disease. N. Engl. J. Med 367, 795–804 (2012). [PubMed: 22784036]
10. Fagan AM et al. Cerebrospinal fluid tau/β-amyloid42 ratio as a prediction of cognitive decline in nondemented older adults. Arch. Neurol 64, 343–349 (2007). [PubMed: 17210801]
11. Vandermeeren M et al. Detection of tau proteins in normal and Alzheimer's disease cerebrospinal fluid with a sensitive sandwich enzyme-linked immunosorbent assay. J. Neurochem61, 1828–1834 (1993). [PubMed: 8228996]
12. Mori H et al. Tau in cerebrospinal fluids: establishment of the sandwich ELISA with antibody specific to the repeat sequence in tau. Neurosci. Lett 186, 181–183 (1995). [PubMed: 7777192]
13. Schindler SE et al. Emerging cerebrospinal fluid biomarkers in autosomal dominant Alzheimer's disease. Alzheimers Dement. 15, 655–665 (2019). [PubMed: 30846386]
14. Toledo JB, Xie SX, Trojanowski JQ & Shaw LM Longitudinal change in CSF Tau and Aβ biomarkers for up to 48 months in ADNI. Acta Neuropathol.126, 659–670 (2013). [PubMed: 23812320]
15. Jack CR Jr. et al. NIA-AA research framework: toward a biological definition of Alzheimer's disease. Alzheimers Dement. 14, 535–562 (2018). [PubMed: 29653606]

16. Jack CR Jr. et al. A/T/N: an unbiased descriptive classification scheme for Alzheimer disease biomarkers. Neurology 87, 539–547 (2016). [PubMed: 27371494]
17. Hu WT et al. Reduced CSF p-Tau181 to Tau ratio is a biomarker for FTLD-TDP. Neurology 81, 1945–1952 (2013). [PubMed: 24174584]
18. Hampel H et al. Measurement of phosphorylated tau epitopes in the differential diagnosis of Alzheimer disease: a comparative cerebrospinal fluid study. Arch. Gen. Psychiatry 61, 95–102 (2004). [PubMed: 14706948]
19. La Joie R et al. Associations between AV1451 tau PET and CSF measures of tau pathology in a clinical sample. Neurology 90, e282–e290 (2018). [PubMed: 29282337]
20. Mattsson N et al. 18F-AV-1451 and CSF T-tau and P-tau as biomarkers in Alzheimer's disease. EMBO Mol. Med 9, 1212–1223 (2017). [PubMed: 28743782]
21. Gordon BA et al. Tau PET in autosomal dominant Alzheimer's disease: relationship with cognition, dementia and other biomarkers. Brain 142, 1063–1076 (2019). [PubMed: 30753379]
22. Jack CR Jr. et al. The bivariate distribution of amyloid-β and tau: relationship with established neurocognitive clinical syndromes. Brain 142, 3230–3242 (2019). [PubMed: 31501889]
23. Johnson KA et al. Tau positron emission tomographic imaging in aging and early Alzheimer disease. Ann. Neurol 79, 110–119 (2016). [PubMed: 26505746]
24. Mattsson N et al. Predicting diagnosis and cognition with 18F-AV-1451 tau PET and structural MRI in Alzheimer's disease. Alzheimers Dement. 15, 570–580 (2019). [PubMed: 30639421]
25. Quiroz YT et al. Association between amyloid and Tau accumulation in young adults with autosomal dominant Alzheimer disease. JAMA Neurol. 75, 548–556 (2018). [PubMed: 29435558]
26. Fleisher AS et al. Associations between biomarkers and age in the presenilin 1 E280A autosomal dominant Alzheimer disease kindred: a cross-sectional study. JAMA Neurol. 72, 316–324 (2015). [PubMed: 25580592]
27. Toledo JB, Xie SX, Trojanowski JQ & Shaw LM Longitudinal change in CSF Tau and Aβ biomarkers for up to 48 months in ADNI. Acta Neuropathol.126, 659–670 (2013). [PubMed: 23812320]
28. Fagan AM et al. Longitudinal change in CSF biomarkers in autosomal-dominant Alzheimer's disease. Sci. Transl. Med 6, 226ra230 (2014).
29. Price JL & Morris JC Tangles and plaques in nondemented aging and "preclinical" Alzheimer's disease. Ann. Neurol 45, 358–368 (1999). [PubMed: 10072051]
30. Ittner LM et al. Dendritic function of Tau mediates amyloid-β toxicity in Alzheimer's disease mouse models. Cell 142, 387–397 (2010). [PubMed: 20655099]
31. Cohen AD et al. Early striatal amyloid deposition distinguishes Down syndrome and autosomal dominant Alzheimer's disease from late-onset amyloid deposition. Alzheimers Dement. 14, 743–750 (2018). [PubMed: 29477284]
32. Maia LF et al. Changes in amyloid-β and Tau in the cerebrospinal fluid of transgenic mice overexpressing amyloid precursor protein. Sci. Transl. Med 5, 194re192 (2013).
33. Sato C et al. Tau kinetics in neurons and the human central nervous system. Neuron 98, 861–864 (2018). [PubMed: 29772204]
34. Schelle J et al. Prevention of tau increase in cerebrospinal fluid of APP transgenic mice suggests downstream effect of BACE1 inhibition. Alzheimers Dement.13, 701–709 (2017). [PubMed: 27750032]
35. Zempel H, Thies E, Mandelkow E &Mandelkow EM Aβ oligomers cause localized Ca2+elevation, missorting of endogenous Tau into dendrites, Tau phosphorylation, and destruction of microtubules and spines. J. Neurosci 30, 11938–11950 (2010). [PubMed: 20826658]
36. Saman S et al. Exosome-associated Tau is secreted in tauopathy models and is selectively phosphorylated in cerebrospinal fluid in early Alzheimer disease. J. Biol. Chem 287, 3842–3849 (2012). [PubMed: 22057275]
37. Jin M et al. Soluble amyloid β-protein dimers isolated from Alzheimer cortex directly induce Tau hyperphosphorylation and neuritic degeneration. Proc. Natl Acad. Sci. USA 108, 5819–5824 (2011). [PubMed: 21421841]

38. Gordon BA et al. Spatial patterns of neuroimaging biomarker change in individuals from families with autosomal dominant Alzheimer's disease: a longitudinal study. Lancet Neurol. 17, 241–250 (2018). [PubMed: 29397305]
39. Ryman DC et al. Symptom onset in autosomal dominant Alzheimer disease: a systematic review and meta-analysis. Neurology 83, 253–260 (2014). [PubMed: 24928124]
40. Morris JC The Clinical Dementia Rating (CDR): current version and scoring rules. Neurology 43, 2412–2414 (1993).
41. Medina M & Avila J Further understanding of tau phosphorylation: implications for therapy. Expert Rev. Neurother 15, 115–122 (2015). [PubMed: 25555397]
42. Benzinger TL et al. Regional variability of imaging biomarkers in autosomal dominant Alzheimer's disease. Proc. Natl Acad. Sci. USA 110, E4502–E4509 (2013). [PubMed: 24194552]
43. Quiroz YT et al. Cortical atrophy in presymptomatic Alzheimer's disease presenilin 1 mutation carriers. J. Neurol. Neurosurg. Psychiatry 84, 556–561 (2013). [PubMed: 23134660]
44. Ridha BH et al. Tracking atrophy progression in familial Alzheimer's disease: a serial MRI study. Lancet Neurol. 5, 828–834 (2006). [PubMed: 16987729]
45. Arriagada PV, Growdon JH, Hedley-Whyte ET & Hyman BT Neurofibrillary tangles but not senile plaques parallel duration and severity of Alzheimer's disease. Neurology 42, 631–639 (1992). [PubMed: 1549228]
46. Okonkwo OC et al. Cerebrospinal fluid profiles and prospective course and outcome in patients with amnestic mild cognitive impairment. Arch. Neurol 68, 113–119 (2011). [PubMed: 21220682]
47. Bateman RJ et al. The DIAN-TU Next Generation Alzheimer's prevention trial: adaptive design and disease progression model. Alzheimers Dement. 13, 8–19 (2017). [PubMed: 27583651]
48. Yanamandra K et al. Anti-tau antibody administration increases plasma tau in transgenic mice and patients with tauopathy. Sci. Transl. Med 9, eaal2029 (2017). [PubMed: 28424326]
49. He Z et al. Amyloid-β plaques enhance Alzheimer's brain tau-seeded pathologies by facilitating neuritic plaque tau aggregation. Nat. Med 24, 29–38 (2018). [PubMed: 29200205]
50. Buerger K et al. CSF phosphorylated tau protein correlates with neocortical neurofibrillary pathology in Alzheimer's disease. Brain 129, 3035–3041 (2006). [PubMed: 17012293]
51. Ittner A et al. Site-specific phosphorylation of tau inhibits amyloid-β toxicity in Alzheimer's mice. Science 354, 904–908 (2016). [PubMed: 27856911]
52. Potter R et al. Increased in vivo amyloid-β42 production, exchange, and loss in presenilin mutation carriers. Sci. Transl. Med 5, 189ra177 (2013).
53. Yamada K et al. In vivo microdialysis reveals age-dependent decrease of brain interstitial fluid tau levels in P301S human tau transgenic mice. J. Neurosci31, 13110–13117 (2011). [PubMed: 21917794]
54. Van der Kant R et al. Cholesterol metabolism is a druggable axis that independently regulates tau and amyloid-β in iPSC-derived Alzheimer's disease neurons. Cell Stem Cell 24, 363–375.e9 (2019). [PubMed: 30686764]

References

55. Morris JC et al. Developing an international network for Alzheimer research: the Dominantly Inherited Alzheimer Network. Clin. Investig. (Lond.) 2, 975–984 (2012).
56. Storandt M, Balota DA, Aschenbrenner AJ & Morris JC Clinical and psychological characteristics of the initial cohort of the Dominantly Inherited Alzheimer Network (DIAN). Neuropsychology 28, 19–29 (2014). [PubMed: 24219606]
57. Lim YY et al. BDNF Val66Met moderates memory impairment, hippocampal function and tau in preclinical autosomal dominant Alzheimer's disease. Brain 139, 2766–2777 (2016). [PubMed: 27521573]
58. McKhann G et al. Clinical diagnosis of Alzheimer's disease: report of the NINCDS-ADRDA Work Group under the auspices of Department of Health and Human Services Task Force on Alzheimer's Disease. Neurology 34, 939–944 (1984). [PubMed: 6610841]

59. Patterson BW et al. Age and amyloid effects on human central nervous system amyloid-beta kinetics. Ann. Neurol 78, 439–453 (2015). [PubMed: 26040676]

60. Del Campo M et al. Recommendations to standardize preanalytical confounding factors in Alzheimer's and Parkinson's disease cerebrospinal fluid biomarkers: an update. Biomark. Med 6, 419–430 (2012). [PubMed: 22917144]

61. Barthelemy NR et al. Tau protein quantification in human cerebrospinal fluid by targeted mass spectrometry at high sequence coverage provides insights into its primary structure heterogeneity. J. Proteome Res 15, 667–676 (2016). [PubMed: 26742856]

62. Su Y et al. Partial volume correction in quantitative amyloid imaging. Neuroimage 107, 55–64 (2015). [PubMed: 25485714]

63. Luo J, D'Angelo G, Gao F, Ding J &Xiong C Bivariate correlation coefficients in family-type clustered studies. Biom. J 57, 1084–1109 (2015). [PubMed: 26360805]

64. Xiong C et al. Longitudinal relationships among biomarkers for Alzheimer disease in the Adult Children Study. Neurology 86, 1499–1506 (2016). [PubMed: 27009258]

65. Benjamini Y & Hochberg Y Controlling the false discovery rate: a practical and powerful approach to multiple testing. J. R. Stat. Soc. B 57, 289–300 (1995).

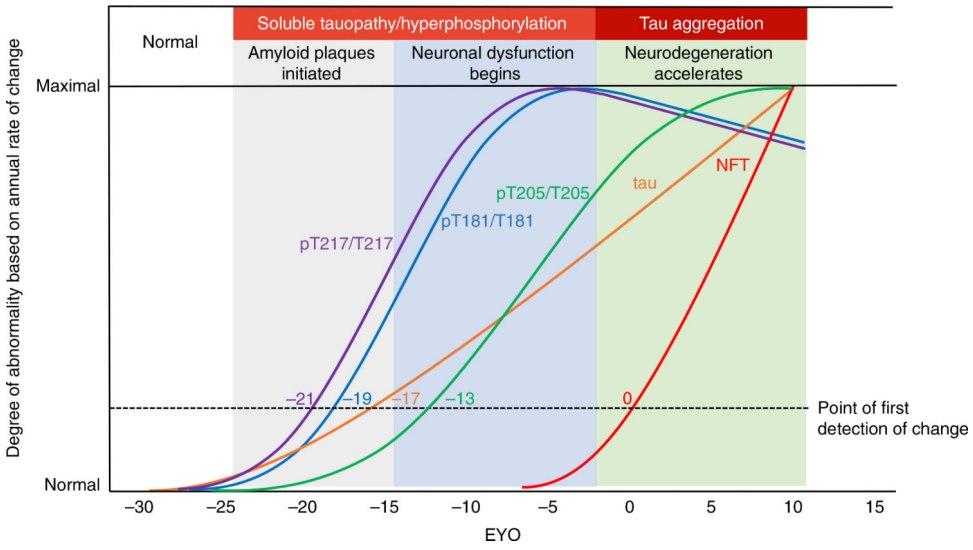

Fig. 1 |. Stages of tau pathology.

Tau pathophysiology evolves through distinct phases in DIAD. Measures of four different soluble tau species and aggregated tau in DIAD show, over the course of 35 years, that tau sequentially changes by stage of disease related to amyloid plaques, cortical atrophy and metabolism. Starting with the development of fibrillar amyloid pathology, levels of pT217 (purple) and pT181 (blue) begin to increase. Then, with the increase in neuronal dysfunction (decreased cortical metabolism), levels of pT205 (green) begin to increase, along with soluble t-tau (orange). Lastly, with the onset of neurodegeneration (based on cortical atrophy and clinical decline), tau-PET tangles (red) begin to develop, while pT217 and pT181 decrease. Together, the dynamic and diverging patterns of soluble and aggregated tau begin in close relationship with amyloid pathology and change over the course of the disease.

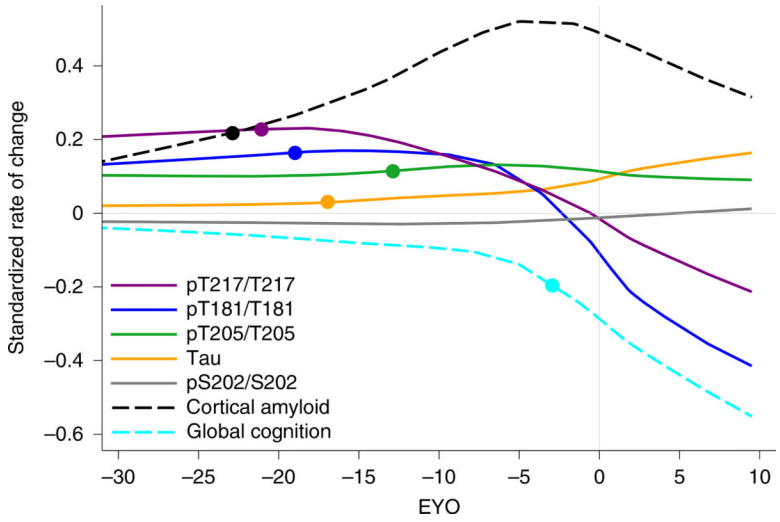

Fig. 2 |. Longitudinal changes of different p-tau sites are specific to disease stage and change in opposite directions as AD progresses in dominantly inherited mutation carriers.

LME model-estimated annual rates of change for each site of phosphorylation, based on the standardized mutation carrier data (n = 370), plotted by EYO along with PiB-PET (black dashed line; n = 304) and cognitive decline (aqua dashed line; n = 356). The solid circles represent the points at which the rate of change for each variable first become different for mutation carriers compared with non-carriers. This highlights the pattern of change for p-tau isoforms over the course of the AD spectrum and the close association between amyloid plaque growth and the increase in pT217/T217, with plaques beginning to increase at −21 EYO and hyperphosphorylation of T217 (purple) also beginning at −21 EYO, followed by an increase in hyperphosphorylation of T181 (blue) at −19 EYO and a decrease in the phosphorylation rate at these two sites associated with a decline in cognition. In contrast, phosphorylation of T205 (green) continues increasing throughout disease progression and t-tau levels (orange) increase at an increased rate near the time of symptom onset. Levels of pS202 do not increase throughout the disease course.

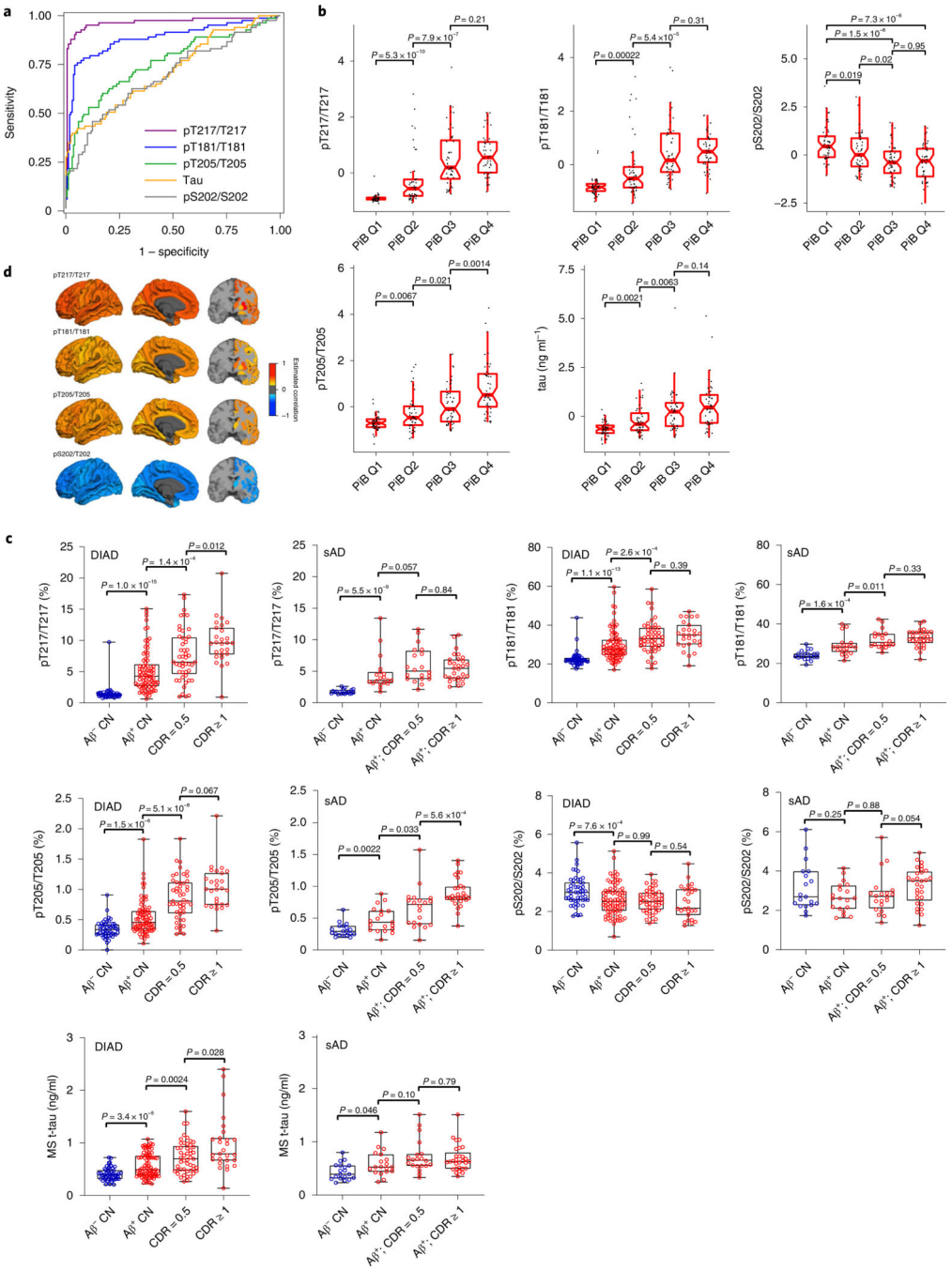

Fig. 3 |. Specific soluble tau phosphorylation sites are differentially associated with amyloid plaques in DIAD and sAD.

a, Receiver operating characteristics of tau phosphorylation with Aß pathology based on Aβ PiB-PET (SUVR cutoff of 1.25) in DIAD (n = 252). There is a near-perfect association with Aβ pathology for pT217/T217 (purple; AUC = 0.97). AUC values for the other phosphorylation ratios were: 0.89 (pT181/T181; blue); 0.74 (pT205/T205; green); 0.72 (t-tau; orange) and 0.69 (pS202/S202; gray). b, Standardized (z score) phosphorylation ratios (pT217/T217, pT181/T181, pS202/S202 and pT205/T205) and t-tau levels by Aβ PiB-PET quartile (n = 47 for Q1; n = 48 for Q2; n = 48 for Q3; n = 48 for Q4) for mutation carriers

suggest site-specific differences in phosphorylation with increasing Aβ PiB-PET levels. pT217, pT181, pT205 and t-tau increase as Aβ PiB-PET increases. There was a significant decrease in the phosphorylation of S202 at the highest Aβ PiB-PET quartiles relative to the lowest (Wilcoxon rank-sum test). **c**, Change in phosphorylation rates and t-tau levels for DIAD ($n = 209$) and sAD ($n = 86$) across the spectrum of clinical progression (blue = cognitively normal/amyloid negative). For DIAD, there is evidence of a higher ratio of phosphorylation, and in both DIAD and sAD, the phosphorylation of T217 and T181 increases once amyloid pathology begins, followed by a plateau. In contrast, pT205 and t-tau levels increase at later stages of disease progression. For S202 in both DIAD and sAD, there is minimal change in the phosphorylation rate across the disease spectrum (Mann–Whitney U-test). For the box plots in **b** and **c**, the middle line represents the median; the upper and lower notches show the median ± 1.58× the interquartile range/square root(number of observations); and the upper (and lower) whiskers represent the largest observation greater (or less than or equal to) the upper (or lower) hinge + 1.58× the IQR. **d**, Cross-sectional, bivariate correlations between cortical and subcortical Aβ PiB-PET SUVR and site-specific phosphorylation for asymptomatic mutation carriers ($n = 152$). Colors represent correlations, with positive correlations in yellow/red and negative correlations in blue. P values for the correlations were derived from a z-test using the covariance matrix of the bivariate LME models. All correlations represent statistically significant values surviving a false discovery rate ($P < 0.05$) with Benjamini–Hochberg correction. They are arranged by correlation strength from top to bottom. CN, cognitively normal; MS, mass spectrometry.

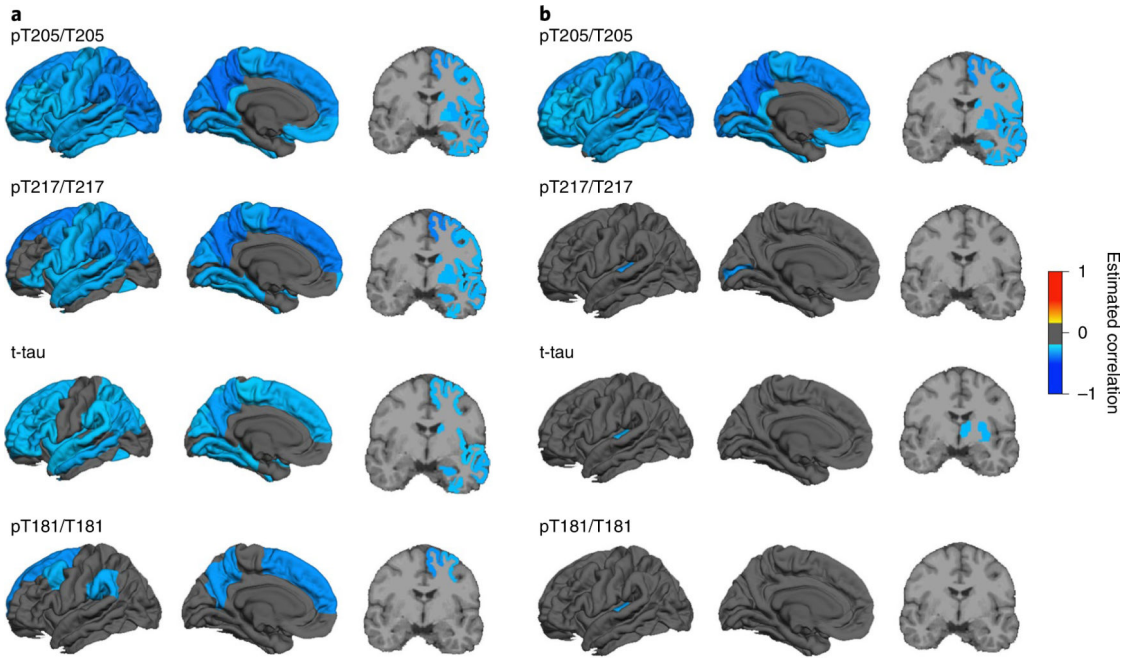

Fig. 4 |. Tau phosphorylation positions are differentially related to brain atrophy and hypometabolism in DIAD.

a, Bivariate correlations between cortical and subcortical atrophy and site-specific phosphorylation ratios in asymptomatic mutation carriers (n = 152) demonstrate an increases in pT205/T205 and pT217/T217, followed by t-tau, and less for pT181/T181. **b**, Bivariate correlations between cortical and subcortical brain metabolism, as measured by FDG-PET, and site-specific phosphorylation ratios in asymptomatic mutation carriers (n = 152) demonstrate an increase in pT205/T205 associated with a decrease in most cortical and subcortical regions, but not for the other p-tau sites or t-tau. P values for the correlations were calculated using chi-squared tests based on the bivariate LME models, with Benjamini–Hochberg correction for multiple comparisons.

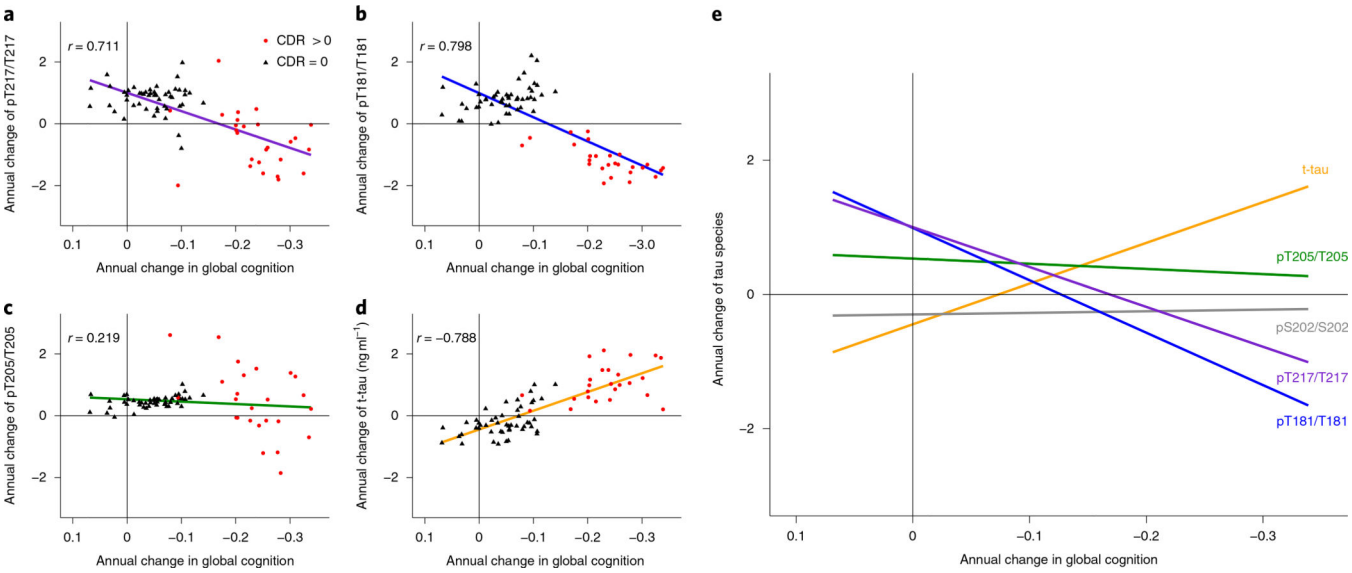

Fig. 5 |. In DIAD, elevated levels of tau phosphorylation decline in some sites with the onset of dementia, in contrast with a continued rise in t-tau.

a–**d**, Individual estimated annualized rates of change of pT217/T217 (**a**), pT181/T181 (**b**), pT205/T205 (**c**) and t-tau (**d**), standardized for all mutation carriers, correlated with the annualized change in global cognitive function. The lines represent simple linear regression and the shaded areas represent 95% CIs. Each point is an individual-level correlation between measures, with Pearson's *r* shown for all data. The linear regression was fit to those with no dementia (CDR = 0; black triangles; $n = 49$) and those with dementia (CDR > 0; red circles; $n = 27$). Declines in pT217/T217 ($r = 0.711$; $P < 0.0001$), pT181/T181 ($r = 0.798$; $P < 0.0001$) and pT205/T205 ($r = 0.219$; $P = 0.06$) were associated with cognitive decline after symptom onset (red). For t-tau, there was an inverse correlation with cognition ($r = -0.788$; $P < 0.0001$). **e**, A linear fit for all mutation carriers demonstrates that there are distinct associations between declining cognition and changes in the different p-tau isoforms and t-tau: with decreases in pT217/T217 and pT181/T181, there is an increase in t-tau associated with cognitive decline, but no associations with pT205/T205 or pS202/S202. This suggests that soluble tau species are not equivalent in AD (pS202/S202 is shown here to demonstrate the lack of association with cognition ($r = -0.09$; $P = 0.39$). Statistical significance for all of the correlations was based on two-sided *t*-test.

Table 1 |

Demographic, CSF, neuroimaging and cognition measures for mutation carriers versus non-carriers and the cohort of non-familial at-risk and symptomatic participants

Cohort with DIAN		**Mutation carriers**		**Mutation non-carriers**	***P* value**
	n [a]	**Asymptomatic (*n* = 152)**	**Symptomatic (*n* = 77)**	**(*n* = 141)**	
Age (years)	370	34.4 ± 8.9	46.2 ± 9.2	38.5 ± 12.2	<0.0001
Female (*n* (%))	370	84 (55.3)	39 (50.7)	88 (62.4)	0.15
Apolipoprotein-E ε4 (*n* (%))	370	48 (31.6)	23 (29.9)	51 (36.2)	0.67
EYO (years)	370	−13.4 ± 8.7	3.42 ± 3.47	−9.2 ± 12.5	<0.0001
Cortical PiB-PET SUVR	304 (133, 50, 121)	1.76 ± 0.89	2.82 ± 1.27	1.06 ± 0.17	<0.0001
PiB^+ (*n* (%)) [b]	304 (133, 50, 121)	81 (60.9)	48 (96.0)	2 (1.65)	<0.0001
CSF pT181/T181	370	26.5 ± 7.2	34.2 ± 7.7	21.7 ± 2.3	<0.0001
CSF pT181 level (ng ml^{-1})	370	0.14 ± 0.09	0.30 ± 0.19	0.088 ± 0.034	<0.0001
CSF pT205/T205	370	0.44 ± 0.24	0.93 ± 0.36	0.34 ± 0.13	<0.0001
CSF pT205 level (ng ml^{-1})	370	0.003 ± 0.003	0.011 ± 0.008	0.002 ± 0.001	<0.0001
CSF pT217/T217	370	3.49 ± 3.08	8.42 ± 4.05	1.25 ± 0.66	<0.0001
CSF pT217 level (ng ml^{-1})	370	0.015 ± 0.018	0.054 ± 0.047	0.004 ± 0.004	<0.0001
CSF pS202/S202	370	2.77 ± 0.80	2.52 ± 0.68	3.10 ± 0.72	<0.0001
CSF pS202 level (ng ml^{-1})	370	0.016 ± 0.006	0.025 ± 0.011	0.014 ± 0.005	<0.0001
CSF tau level (ng ml^{-1})	370	0.51 ± 0.21	0.82 ± 0.41	0.40 ± 0.14	<0.0001
Precuneus (mm)	344 (146, 64, 134)	2.37 ± 0.15	2.10 ± 0.24	2.38 ± 0.14	<0.0001
Cortical FDG-PET SUVR	318 (137, 59, 122)	1.73 ± 0.14	1.57 ± 0.18	1.71 ± 0.14	<0.0001

Hippocampal volume (mm^3)	344 (146, 64, 134)	8,863 ± 970	7,290 ± 1214	8,787 ± 775	<0.0001
Cognitive composite (*z* score)	356 (151, 66, 139)	−0.096 ± 0.640	−1.67 ± 0.85	−0.03 ± 0.59	<0.0001
At-risk and sAD cohort					
	n [c]	**Amyloid negative (*n* = 39)**	**Amyloid positive**		
			Asymptomatic (*n* = 18)	**Symptomatic (*n* = 45)**	***F* value** [d]
Age (years)	102	73.3 ± 8.6	71.6 ± 6.4	72.6 ± 6.2	0.41
Female (*n* (%))	102	17 (44)	8 (44)	31 (69)	0.041 (*P* value)
MMSE score	102	28.7 ± 1.6	29.4 ± 0.5	23.6 ± 3.9	45.44***
CSF pT181/T181	102	13.8 ± 1.3	16.6 ± 2.9	18.8 ± 2.5	53.55***
CSF pT205/T205	102	0.14 ± 0.06	0.2 ± 0.08	0.33 ± 0.11	50.6***
CSF pT217/T217	102	3.3 ± 1.4	8.2 ± 4.8	10 ± 4.1	39.18***
CSF pS202/S202	102	1.4 ± 0.48	1.2 ± 0.33	1.38 ± 0.45	1.042
CSF tau level (ng ml^{-1})	102	0.76 ± 0.31	0.89 ± 0.32	1.1 ± 0.41	7.14**

Continuous measures are presented as means ± s.d. For mutation carriers and non-carriers, the significance of the difference among asymptomatic mutation carriers, symptomatic mutation carriers and non-carriers was calculated using a *t*-test based on an LME model (for continuous outcomes) and a generalized LME model with a logistic link (for categorical outcomes). All of the mixed models included a random family effect to account for the correlations on the outcome measures between participants within the same family. For the non-familial at-risk and symptomatic cohort, the *P* values were calculated by one-way analysis of variance (for continuous outcomes) and chi-squared test (for categorical outcomes).

[a] Total number of participants, with numbers of asymptomatic mutation carriers, symptomatic mutation carriers and non-carriers, respectively, in parentheses).

[b] PiB^+ = standard uptake value ratio (SUVR) > 1.25.

[c] Total number of amyloid-negative and amyloid-positive (asymptomatic and symptomatic) participants.

[d] ** *P* = 0.01

*** *P* = 0.001.

All other *F* values had a *P* value > 0.05. MMSE, mini-mental state examination; p, phosphorylated; S, serine; T, threonine.